NASA TECHNICAL NOTE

NASA TN D-4950
C. 1

EXPERIMENTAL OBSERVATION OF
OSCILLATIONS DESCRIBED BY
THE CONTINUITY EQUATIONS
OF SLIGHTLY IONIZED
DEUTERIUM, NEON, AND HELIUM GAS

by J. Reece Roth

Lewis Research Center
Cleveland, Ohio

NASA TN D-4950

EXPERIMENTAL OBSERVATION OF OSCILLATIONS DESCRIBED BY

THE CONTINUITY EQUATIONS OF SLIGHTLY IONIZED

DEUTERIUM, NEON, AND HELIUM GAS

By J. Reece Roth

Lewis Research Center
Cleveland, Ohio

NATIONAL AERONAUTICS AND SPACE ADMINISTRATION

ABSTRACT

Low-frequency oscillations in the electron number density of a slightly ionized gas have been observed in deuterium, neon, and helium over the frequency range from 10^2 to 8×10^4 Hz. These oscillations can be identified with periodic solutions to the neutral- and charged-particle continuity equations. The observed functional dependence of the waveform and of the peak-to-peak amplitude of the oscillation are qualitatively consistent with this mechanism. The frequency of the oscillation was independent of magnetic field strength and had the predicted square-root dependence on the product of electron and neutral number density $\left(\nu \sim \sqrt{\tilde{n}_e n_o} \right)$.

CONTENTS

EXPERIMENTAL OBSERVATION OF OSCILLATIONS DESCRIBED BY
THE CONTINUITY EQUATIONS OF SLIGHTLY IONIZED
DEUTERIUM, NEON, AND HELIUM GAS

by J. Reece Roth

Lewis Research Center

SUMMARY

This report presents the first series of systematic experimental measurements which has been made on the oscillation mechanism described by the neutral- and charged-particle continuity equations. Low-frequency oscillations in the electron number density of a slightly ionized gas have been observed in deuterium, neon, and helium over the frequency range from 10^2 to 8×10^4 hertz.

A brief outline is presented of the physical mechanism responsible for this oscillation. It is demonstrated that a small-amplitude approximation can be applied to the equations of continuity for neutrals and charged particles. A closed-form solution is obtained for periodic oscillations of the charged-particle number density. These periodic solutions are given in terms of Jacobian elliptic functions and predict the functional dependence of the frequency, waveform, and peak-to-peak amplitude on the experimental variables. These predicted functional relations are used to compare the theory with experimental observations. It is characteristic of these oscillations that the frequency, waveform, and amplitude of the oscillations in charged-particle number density are determined only by the initial conditions and the coefficients of the terms in the continuity equations. The equations for conservation of energy and momentum are, of course, satisfied but play no direct role in determining the waveform of $n_e(t)$.

The observed functional dependence of the waveform and of the peak-to-peak amplitude on the experimental variables are qualitatively consistent with the continuity-equation oscillation mechanism. The frequency of the oscillation was observed to be independent of magnetic field strength, as predicted, over more than a factor of 2 variation in the magnetic field and to have the predicted square-root dependence on the product of electron and neutral number density $\left(\nu \sim \sqrt{\tilde{n}_e n_o} \right)$. The existence and operation of the continuity-equation oscillation mechanism has been demonstrated over more than five orders of magnitude in the product $\tilde{n}_e n_o$.

INTRODUCTION

Plasmas in magnetic fields are subject to oscillatory phenomena of many kinds, which occur over a wide range of frequencies. These phenomena include both propagating waves and bulk oscillatory plasma instabilities. The literature on this subject is much too extensive to cite here completely or in detail. A comprehensive review has been given by Lehnert (ref. 1) of those plasma oscillations relevant to controlled-fusion research.

Much of the interest in plasma oscillations has been focused on the higher-frequency range which encompasses the ion and electron cyclotron frequencies or the electron or ion plasma frequencies. In normal experimental situations, these frequencies range from 10^6 to more than 10^{11} hertz. The low-frequency range, below 10^6 hertz, is less often the subject of careful investigation. Plasma oscillations in this range have been observed, but are usually ascribed to "turbulence" or bulk motion of the plasma arising from $\underline{\mathcal{E}} \times \underline{B}$ rotational instabilities. (All symbols are defined in appendix A.)

In November 1966, the author observed coherent oscillations in a modified Penning discharge (ref. 2) over the frequency range from 10^2 to 10^5 hertz. The frequency of the oscillations was a function of both the electron and neutral number densities and was independent of the magnetic field strength over more than a factor of 2 variation in this quantity. The observed characteristics ruled out known oscillatory mechanisms and led to the formulation of a theory of plasma oscillation based on the neutral- and charged-particle continuity equations (ref. 3).

A qualitatively similar mechanism was suggested by H. S. Robertson (ref. 4) as a possible explanation of moving striations in classical gaseous discharge tubes. He suggested that moving striations result from traveling-wave periodic solutions to the spatially inhomogeneous charged-particle and metastable-atom (rather than neutral particle) continuity equations. Because Robertson retained the spatially dependent diffusion terms in his continuity equations, the resulting dispersion relation was too complicated to be solved for any but highly specialized limiting cases. Robertson's formulation of the problem was retained by K. W. Gentle (ref. 5), who obtained computer solutions to the continuity equations for a particular application involving argon gas.

The conditions of the present experiment were such that the neutral-neutral mean free path was much longer, and the Debye distance shorter, than the apparatus dimensions. The oscillations of the discharge were observed with a pair of collimated photomultipliers which were placed at several axial and azimuthal positions. It was found that the discharge was oscillating in unison, with a single phase and frequency. These observations indicated that diffusion processes were not too important in determining the dynamics of the discharge or the characteristics of the oscillation. The spatially dependent diffusion terms were therefore omitted from the continuity equations.

The continuity equations for the conservation of neutral and charged particles in a plasma constitute a coupled set of at least two first-order nonlinear differential equations. General, closed-form solutions to these equations are not available. Lotka (ref. 6) and Volterra (ref. 7) solved a simplified pair of coupled equations by using a small-perturbation approach, in which it was assumed that the peak-to-peak amplitude of both variables was small by comparison with their mean values. This approach enabled these authors to obtain an expression for the frequency as a function of the coefficients of the terms in the continuity equations. However, they were not able to obtain an expression for the peak-to-peak amplitude of the oscillations as a function of these coefficients, nor was it possible for them to study the waveform of the oscillations in the nonlinear limit of large relative peak-to-peak amplitudes.

In references 8 and 9, the author has presented a family of closed-form periodic solutions to a pair of generalized spatially uniform continuity equations. These solutions give the frequency, waveform, and peak-to-peak amplitude as functions of the coefficients of the terms of the equations. The latter are determined by the experimental conditions. The general analysis contained in references 8 and 9 was specialized to conform to the particular situation existing in the present experiment. This specialized analysis is described in reference 3. The present study includes the experimental measurement of the characteristics of these plasma oscillations over a wide range of operating conditions with deuterium, neon, and helium gas. These experiments were intended to explore the range of validity of the oscillation model previously developed.

THEORETICAL ANALYSIS

Physical Mechanism of Oscillations

Several entirely distinct physical models are capable of yielding a coupled pair of continuity equations, without diffusion terms, that possess periodic solutions. A model that appears appropriate to the present experiment is shown schematically in figure 1. It is assumed that the discharge is populated by charged particles sufficiently energetic to ionize the neutral gas. The neutral gas in the vacuum system can be conceptually divided into two categories: (1) neutral gas that circulates through the discharge without being ionized, shown at the top of figure 1, and (2) an average fraction α of this recirculating flux of neutrals that interacted in the discharge volume by electron-neutral ionization during a previous cycle of the oscillation. The electrons and ions produced in the discharge volume are lost to the walls, where they recombine, and these recombined neutrals then find their way back to the discharge.

It is important to note that at any instant of time there is not a detailed balance
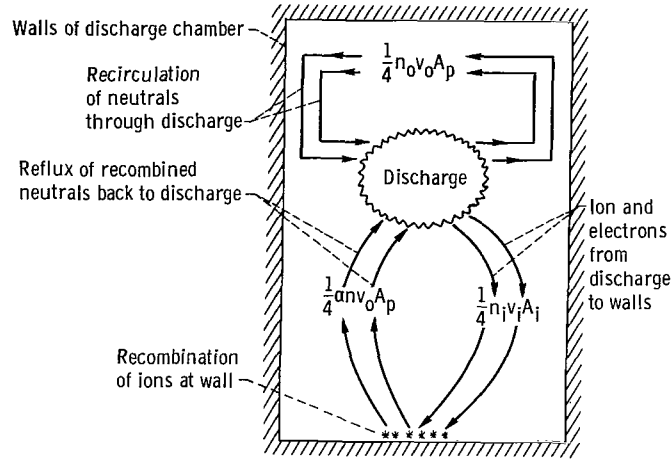
Figure 1. - Schematic drawing of discharge in vacuum tank. Neutral gas circulates through discharge, and an average fraction α is ionized.

between the oscillating flux of **charged particles** leaving the discharge and the virtually constant flux of recombined neutrals entering. The time delay associated with the transit of the particles within the discharge volume acts as an averaging mechanism that prevents a detailed balance, and makes possible a relaxation oscillation of the charged-particle number density in the discharge. In the present experiment, the magnetic field lines on which the charged particles are confined intersect the vacuum-tank walls about 80 centimeters from the discharge. The experimental geometry depicted in figure 1 occurs frequently in practice, particularly in fusion-research apparatus, and it would therefore not be surprising to find that this type of relaxation oscillation is quite prevalent.

An analysis of an alternative physical model for this oscillation is presented in appendix B. This model depends on the averaging effect of time delays associated with neutral transport across the discharge and yields the same pair of continuity equations as the model shown in figure 1. The model contained in appendix B is appropriate to situations, like the present experiment, in which Fick's law is not valid.

Equations of Continuity

Under the present experimental conditions, the Debye distance was much smaller than the discharge dimensions (≈ 5 cm) over virtually the entire range of operation. This fact can be used to justify the assumption of quasi-neutrality $n_i \approx n_e$ and makes it possible to eliminate one of the two charged-particle continuity equations from consideration. The neutral- and charged-particle continuity equations appropriate to the situation depicted in figure 1 are

4

$$\dot{n} = \frac{\alpha n v_o A_p}{4V} - n n_e \langle \sigma v \rangle_{ne} \qquad (1)$$

and

$$\dot{n}_e = -\frac{n_e v_i A_i}{4V} + n n_e \langle \sigma v \rangle_{ne} \qquad (2)$$

where the assumption of quasi-neutrality has been used to set $n_i = n_e$ in equation (2). The symbols used are defined in appendix A. A verification of equation (1) is given in appendix B for the slab geometry.

The first term in equation (1) is the average fraction α of the total neutral flux through the discharge that interacted in the discharge volume during a previous cycle of the oscillation. This neutral gas is assumed to flow with a velocity v_o into a discharge of volume V across a plasma-vacuum boundary surface of area A_p. It is shown in appendix B that this term can also be written as a function of the average electron number density in the discharge

$$\frac{\alpha v_o A_p}{4V} = \tilde{n}_e \langle \sigma v \rangle_{ne} \qquad (3)$$

where $\tilde{n}_e$ is the electron number density averaged over one cycle of oscillation. Equation (3) is a consequence of the average net number of neutrals ionized being equal to the average net number of ions produced over a cycle of oscillation.

The second terms in equations (1) and (2) account for the loss of neutrals and the production of ions by an ionization process with the rate coefficient $\langle \sigma v \rangle_{ne}$. This rate coefficient may depend on the electron energy. It is assumed that the energy of the ionizing particles, and hence of $\langle \sigma v \rangle_{ne}$, does not vary over a cycle of oscillation.

The first term in equation (2) represents the efflux of ions of velocity v_i across the appropriate discharge boundary surface of area A_i. The latter area can be taken as the area normal to the magnetic field lines at the maximum magnetic field in the present experiment. This loss rate is that which would result if a Maxwellianized gas were confined in a box and were then permitted to leak out a small hole of area A_i. The validity of this assumption must be tested by comparing the predictions based on it with the experimental results; it is an encouraging fact, however, that the charged particles within the discharge of the present experiment were found to be Maxwellian to a good approximation for all but certain of the runs with helium gas.

If collisions between neutral and charged particles result in the loss of the charged particles, as by knocking them into an escape cone in velocity space, the rate coef-

ficient in equation (2) would have to be reduced accordingly to reflect this process. If collisions of two charged particles result in one of them being knocked into an escape cone, a term proportional to n_e^2 should then be added to equation (2). Charge-exchange processes may be accounted for by appropriate modification of the terms of equation (1). Such processes, however, should not be important in the present experiment.

Periodic Small-Amplitude Solutions

In reference 8 it is shown that closed-form solutions to equations (1) and (2) can be obtained in the small-amplitude limit

$$n(t) = n_o + \delta n(t) \tag{4}$$

in which the peak-to-peak amplitude of the neutral density is much smaller than the average neutral density,

$$\delta n(t) \ll n_o \tag{5}$$

Inequality (5) is satisfied in the present experiment, since the gas is only slightly ionized, and $\delta n(t)$ should not be significantly larger than the charged-particle density. The mathematical development of reference 3 is given below for the convenience of the reader, from equation (6) to equation (22).

A closed-form expression for $n_e(t)$ can be obtained by differentiating equation (2) with respect to time and then removing $\dot{n}$ and $\dot{n}_e$ by substituting equations (1) and (2) to obtain

$$\ddot{n}_e = \left(n\langle\sigma v\rangle_{ne} - \frac{v_i A_i}{4V} \right)^2 n_e + \frac{\alpha n v_o A_p \langle\sigma v\rangle_{ne}}{4V} n_e - n\langle\sigma v\rangle_{ne}^2 n_e^2 \tag{6}$$

If the following initial conditions are applied

$$n(0) \equiv n_o \tag{7a}$$

$$n_e(0) \equiv n_{eo} \tag{7b}$$

$$\dot{n}_e(0) \equiv 0 \tag{7c}$$

with n_{eo} an extremal value of $n_e(t)$, the definition of n_o and $\dot{n}_e(0)$ implies with equation (2) that

$$\left(n_o \langle \sigma v \rangle_{ne} - \frac{v_i A_i}{4V} \right) = 0 \tag{8}$$

If the small-amplitude approximation $n(t) = n_o + \delta n(t)$ is substituted into equation (6), the coefficients of $n_e(t)$ and $n_e^2(t)$ can be separated into two groups, large constant terms containing n_o and smaller time-dependent terms containing $\delta n(t)$. Under a wide range of interesting experimental conditions the behavior of $n_e(t)$ will be dominated by the large constant terms in the coefficients containing n_o and only slightly perturbed by the small time-dependent terms containing $\delta n(t)$. The small-amplitude approximation $n_o \gg \delta n(t)$ therefore allows the coupled equations (1) and (2) containing $n(t)$ and $n_e(t)$ to be approximated by an equation in a single variable, $n_e(t)$. Among the terms omitted is one that is negligible only if

$$\frac{\delta n(t)}{n_o} \ll \frac{n_{eo} - n_e(t)}{\delta n(t)} \equiv \frac{\delta n_e(t)}{\delta n(t)} \tag{9}$$

This inequality will not hold during that portion of the waveform for which $\delta n_e(t) \approx 0$. However, it should hold at other times, since

$$\left| \delta n_e \right|_{max} \approx \left| \delta n \right|_{max} \tag{10}$$

This order-of-magnitude equality can be expected to hold, since the ionization process implies a one-to-one relation between neutrals lost and electrons gained. The effects of neglecting this and other second-order terms is discussed when the small-amplitude approximation is compared with the exact solutions to equations (1) and (2) which were obtained on an analog computer. With the aid of equation (8), an equation in the single variable $n_e(t)$ can be written.

$$\ddot{n}_e = \frac{\alpha n_o v_o A_p \langle \sigma v \rangle_{ne}}{4V} n_e - n_o \langle \sigma v \rangle_{ne}^2 n_e^2 \tag{11}$$

Equation (11) is recognizable as a nonlinear equation with closed-form solutions that may be expressed in terms of Jacobian elliptic functions (refs. 10 and 11).

By using the methods described in reference 8, equation (11) may be solved by

integrating twice and using either expression 235:00 or 236:00 in reference 11. In expressing the solutions of equation (11), it is convenient to define the dimensionless variable

$$\eta \equiv \frac{\alpha v_o A_p}{4 V n_{eo} \langle \sigma v \rangle_{ne}} = \frac{\tilde{n}_e}{n_{eo}} \tag{12}$$

where the second equality follows from the discussion of appendix B. Also define

$$Z_2 \equiv -\frac{3}{4} \left[(2 - \eta) + \sqrt{\left(\eta - \frac{2}{3}\right)(\eta + 2)} \right] \tag{13}$$

and

$$Z_3 \equiv -\frac{3}{4} \left[(2 - \eta) - \sqrt{\left(\eta - \frac{2}{3}\right)(\eta + 2)} \right] \tag{14}$$

When the parameter η lies in the range $2/3 \le \eta \le 1$, a solution to equation (11) may be written (ref. 8)

$$n_e(t) = n_{eo} \left\{ 1 + Z_3 SN^2 \left[2K(k) \nu t \right] \right\} \tag{15}$$

where SN is the Jacobian elliptic sine, $K(k)$ is the complete elliptic integral of the first kind, n_{eo} in this equation is the maximum electron density, and k^2 is the elliptic modulus

$$k^2 = \frac{Z_3}{Z_2} \tag{16}$$

The peak-to-peak amplitude of the oscillations is equal to Z_3, and the frequency is

$$\nu = \frac{\langle \sigma v \rangle_{ne} \sqrt{n_o n_{eo}}}{2\pi} G(\eta) \tag{17}$$

where n_o and n_{eo} can be approximated by the time- and space-averaged number densities, and the parameter $G(\eta)$ is given by

$$G(\eta) = \frac{\pi}{2K(k)} \left(-\frac{2Z_2}{3} \right)^{1/2} \qquad (18)$$

When the parameter $\eta \geq 1$, the solution to equation (11) is given by (ref. 3),

$$n_e(t) = n_{eo} \left\{ 1 + \frac{Z_2 Z_3 SN^2 \left[2K(k)\nu t \right]}{Z_2 - Z_3 + Z_3 SN^2 \left[2K(k)\nu t \right]} \right\} \qquad (19)$$

where n_{eo} is now the minimum value of the electron density. The elliptic modulus k^2 is given by

$$k^2 = \frac{Z_3}{Z_3 - Z_2} \qquad (20)$$

The peak-to-peak amplitude is again given by Z_3, and the frequency of the oscillations by

$$\nu = \frac{\langle \sigma v \rangle_{ne} \sqrt{n_{eo} n_o}}{2\pi} H(\eta) \qquad (21)$$

where the parameter $H(\eta)$ is given by

$$H(\eta) = \left[\left(\eta - \frac{2}{3} \right)(\eta + 2) \right]^{1/4} \frac{\pi}{2K(k)} \qquad (22)$$

Characteristics of Solutions

The waveform of the solutions for $n_e(t)$ over the range $1.0 \leq \eta \leq \infty$ is shown in figures 2(a) to (c) for three values of η. The waveforms in figure 2 represent equation (19) as a function of the argument. The maximum values were normalized to 1. It is clear from figure 2 that the waveform of $n_e(t)$ is approximately sinusoidal in the vicinity of $\eta = 1.0$, but as η approaches the end of its range, the waveform takes on the cuspoid shape characteristic of Jacobian elliptic functions, with broad, shallow minima between sharp, narrow peaks. The waveforms of $n_e(t)$ are shown in appendix C over the entire range $2/3 \leq \eta \leq \infty$.
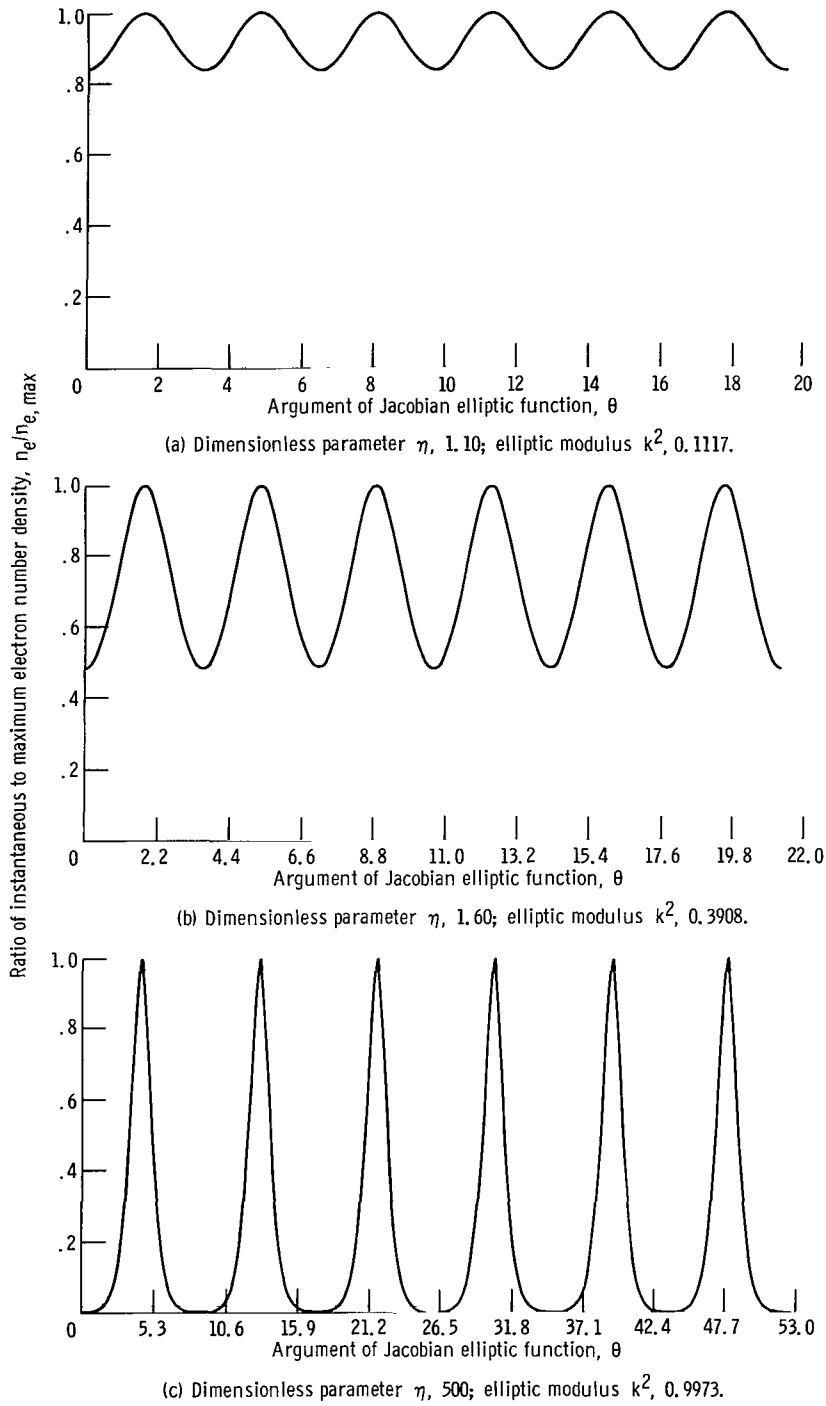
9

(a) Dimensionless parameter η, 1.10; elliptic modulus k^2, 0.1117.

(b) Dimensionless parameter η, 1.60; elliptic modulus k^2, 0.3908.

(c) Dimensionless parameter η, 500; elliptic modulus k^2, 0.9973.

Figure 2. – Normalized graphs of equation (19) ($\eta \geq 1.0$) as functions of argument $\theta = 2K(k)\nu t$. (Note increase in peak-to-peak amplitude and characteristic Jacobian waveform as η approaches end of its range. When $\eta = 1.0$, eqs. (1) and (2) represent a nonoscillating steady state.)

An examination of equations (18) and (22) shows that when η is in the vicinity of 1.0, $H(\eta) \approx G(\eta) \approx 1.0$, and the frequency of oscillation is approximately given by

$$\nu \approx \frac{\langle \sigma v \rangle_{ne} \sqrt{\tilde{n}_e n_o}}{2\pi} \qquad (n \approx 1.0) \qquad (23)$$

This approximation is useful for values of η near 1. Limitations of the experimental arrangement made it impossible to calculate $G(\eta)$ and $H(\eta)$. It was therefore necessary in reducing the experimental data to treat equation (23) as if it held exactly.

The factors $G(\eta)$ and $H(\eta)$ come into play because a peak-to-peak cycle of oscillation of the Jacobian elliptic functions occupies $2K(k)$ radians. This is equal to π radians only in the limit $k^2 = 0$, which occurs at $\eta = 1.0$. The behavior of $G(\eta)$ and $H(\eta)$ as functions of the parameter η is shown in figures 3(a) and (b), respectively. The frequency of the oscillations given by equations (17) and (21) is a function of their amplitude, as would be expected from the nonlinear nature of the original differential equations.

An examination of equations (15) and (19) for $n_e(t)$ shows that the ratio of the peak-to-peak amplitude to the maximum value $n_{e,max}$ is given by

$$\frac{\Delta n_e}{n_{e,max}} = -z_3 \qquad (24)$$

over the range $2/3 \leq \eta \leq 1.0$, and by

$$\frac{\Delta n_e}{n_{e,max}} = \frac{z_3}{z_3 + 1} \qquad (25)$$

for $\eta \geq 1.0$. The behavior of the peak-to-peak amplitude as a function of η is illustrated in figure 3. Equation (24) is plotted in this figure for $\eta \geq 1.0$, and equation (25) for $\eta \geq 1.0$. As η is varied over its range, the peak-to-peak amplitude is equal to the maximum value at $\eta = \infty$, decreases monotonically to 0 at $\eta = 1.0$, and then again becomes equal to the maximum value at $\eta = 2/3$.

The behavior of the elliptic modulus k^2 as a function of η is also shown in figure 3. Equation (16) is plotted for the range $2/3 \leq \eta \leq 1.0$, and equation (20) for $\eta \geq 1.0$. When $k^2 = 0$, the Jacobian elliptic sine becomes identical to the conventional trigonometric sine.

A nondimensional form of equations (1) and (2) was programmed on an analog com-
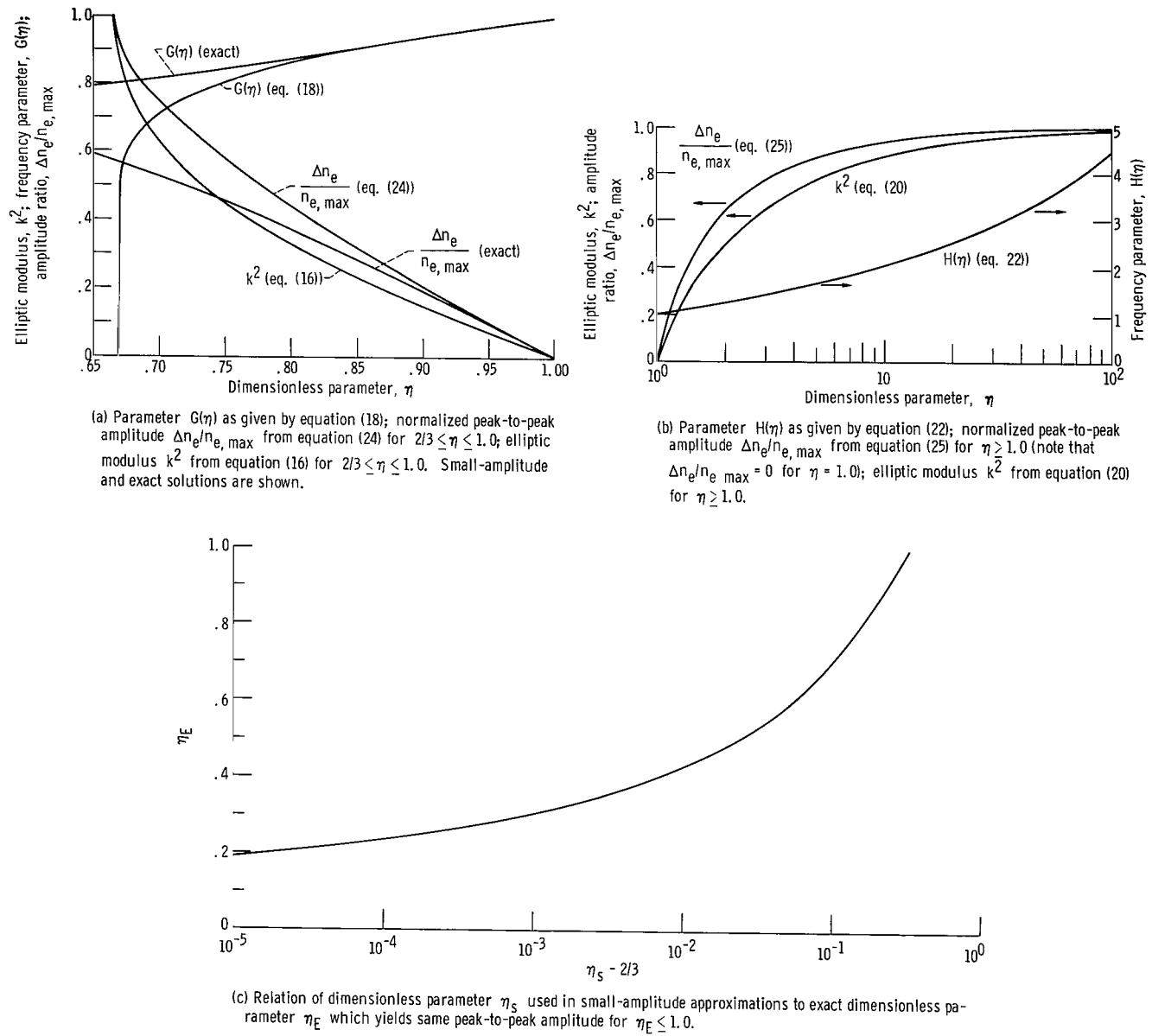
(a) Parameter $G(\eta)$ as given by equation (18); normalized peak-to-peak amplitude $\Delta n_e/n_{e,\,max}$ from equation (24) for $2/3 \leq \eta \leq 1.0$; elliptic modulus k^2 from equation (16) for $2/3 \leq \eta \leq 1.0$. Small-amplitude and exact solutions are shown.

(b) Parameter $H(\eta)$ as given by equation (22); normalized peak-to-peak amplitude $\Delta n_e/n_{e,\,max}$ from equation (25) for $\eta \geq 1.0$ (note that $\Delta n_e/n_{e\,\,max} = 0$ for $\eta = 1.0$); elliptic modulus k^2 from equation (20) for $\eta \geq 1.0$.

(c) Relation of dimensionless parameter η_s used in small-amplitude approximations to exact dimensionless parameter η_E which yields same peak-to-peak amplitude for $\eta_E \leq 1.0$.

Figure 3. - Frequency parameters, normalized peak-to-peak amplitude, and elliptic modulus as functions of dimensionless parameter η, for exact and small-amplitude solutions.

puter to ascertain how the exact solutions so obtained compared with equation (15), which is based on the small-amplitude approximation. For the specific conditions examined, the latter equation was a satisfactory approximation in the range $0.80 \leq \eta \leq 1.0$. The exact solutions were more oscillatory than predicted by the small-amplitude approximation, since oscillatory behavior was observed at values of η as low as 0.21, rather than cutting off at $\eta = 2/3$. The waveforms of $n_e(t)$ obtained from the exact solution as η varied over the range $0.21 \leq \eta \leq 1.0$ displayed all the qualitative features predicted by equation (15) as η varied over the range $2/3 \leq \eta \leq 1.0$, including the sharply peaked maxima with broad, flat minima. The exact analog computer solution of $\Delta n_e/n_{e,max}$ and $G(\eta)$ for $\eta \leq 1.0$ are shown in figure 3(a) to illustrate the region of validity of the small-amplitude approximation.

The useful range of the small-amplitude approximation can be extended below $\eta = 0.80$ by taking the "actual" value of η, given by equation (12), and replacing it by the "small-amplitude-equivalent" value of η in equations (13) to (22). The actual value of η, η_e, (which can vary over at least the range $0.21 \leq \eta_e \leq 1.0$) is related to the small-amplitude-equivalent value of η, η_s, (which is restricted to the range $2/3 \leq \eta_s \leq 1.0$) by the mapping shown on figure 3(c). The equivalent value of η was obtained by requiring that the peak-to-peak amplitude of the exact solutions from the analog computer (for a given actual η) be the same as the peak-to-peak amplitude of $n_e(t)$ for the small-amplitude-equivalent value of η. The latter is plotted along the abscissa of figure 3(c) as $(\eta_s - 2/3)$, because of the compression of the small-amplitude solutions near the point $\eta = 2/3$.

Predictions for Experimental Check

If the observed oscillations are to be explained by this theory, the basic requirements for the oscillation process and the observable features which can be compared with theoretical predictions must be known. In the first place, the continuity equations as written (eqs. (1) and (2)) must correctly represent the processes active in the discharge. The production rate of charged particles must depend only on the product of electron and neutral number density, and the ionization-rate coefficient must not be a function of time. The loss and influx rates of charged and neutral particles must also be correctly represented by the linear terms used. If these restrictions on the processes in the discharge are satisfied, the oscillations should be seen to follow the relations given by equations (15) or (19), within the limitations imposed by the small-amplitude approximation used.

The magnetic field strength B does not appear in equations (1) and (2), and it follows that the frequency, waveform, and other features of the oscillation should not

depend explicitly on the magnetic field strength. However, if there is an implicit dependence of the electron number density, neutral number density, or of $\langle\sigma v\rangle_{ne}$ on magnetic field, the characteristics of these oscillations will be a function of the magnetic field. Oscillation frequency should be an explicit function of magnetic field only when a magnetic-field-dependent diffusion term appears in the continuity equations, as it would in discharge tubes of the kind treated by Robertson (ref. 4). The expected independence of frequency of magnetic field strength is in contrast to the oscillations and fluctuations governed by the momentum equation, where $\underline{v} \times \underline{B}$ forces usually result in an explicit dependence of frequency on magnetic field strength.

A second experimental check of the theory is the observation of a waveform of $n_e(t)$ which varies in a manner resembling that shown in figure 2 and appendix C. Particularly significant would be the observation of cusped waveforms, with sharp peaks and broad, flat minima. Such waveforms are characteristic of Jacobian elliptic functions with values of k^2 near 1. If the experimental conditions are such that $k^2 \approx 0$, the waveform of $n_e(t)$ will be nearly sinusoidal and a convincing check based on the cusp-like waveform of $n_e(t)$ will not then be possible.

A third experimental check of the theory can be provided by varying the experimental parameters over their range and observing whether the peak-to-peak amplitude of $n_e(t)$ varies with η in the manner shown in figure 3. The peak-to-peak amplitude should have large values at either end of the range of η and should be zero for some intermediate value of η. The parameter η, given by equation (12), can be written in terms of experimental variables by multiplying both numerator and denominator by $n_0 \langle\sigma v\rangle_{ne}$ and then assuming that the observed frequency is given by equation (23) for η not near the ends of its range, so that

$$\eta \equiv \frac{\alpha n_o v_o A_p \langle\sigma v\rangle_{ne}}{4 V n_{eo} n_o \langle\sigma v\rangle_{ne}^2} \approx \frac{\alpha n_o v_o A_p \langle\sigma v\rangle_{ne}}{16\pi^2 V \nu_{obs}^2} \tag{26}$$

The average anode current to the discharge used in the present experimental apparatus is approximately given by

$$I_a \approx \frac{\alpha n_o v_o A_p e}{4} \tag{27}$$

since this is the average total flux of charged particles from the discharge. The relevant mean free paths were too long for recombination to have occurred and affected equation (27), and it was observed that very few electrons were lost with the ions out the ends of the discharge. Virtually all electrons seem to have left the discharge across

14

the anode sheath. Equation (27) can be used to write η in terms of the anode current I_a and the observed oscillation frequency ν_{obs}

$$\eta \approx \frac{I_a \langle \sigma v \rangle_{ne}}{e 4 \pi^2 V \nu_{obs}^2} \tag{28}$$

In the experimental conditions of interest in this paper, $\langle \sigma v \rangle_{ne}$ and the plasma volume V will be approximately constant during a series of experimental runs.

A fourth experimental check of the theoretical model can be provided by experimentally varying the charged-particle and neutral number density and plotting the measured frequency as a function of the product of these two quantities, $\tilde{n}_e n_0$. If the frequency is given by equation (23), consistent with the continuity-equation mechanism, a log-log plot of ν as a function of $\tilde{n}_e n_0$ should reveal a square-root dependence on the latter quantity, a straight line of slope $1/2$. If the ion or electron energy also changes while $\tilde{n}_e$ and/or n_0 are varied, the square-root dependence of ν on the product $\tilde{n}_e n_0$ might be complicated by an energy dependence of the ionization-rate coefficient $\langle \sigma v \rangle_{ne}$. However, it is reasonable to hope that $\langle \sigma v \rangle_{ne}$ might be approximately constant over a wide range of $\tilde{n}_e$ and n_0, since for many gases this quantity varies by no more than a few tens of percent over more than an order of magnitude in electron energy.

When the quantity $\langle \sigma v \rangle_{ne}$ does vary significantly during a set of experimental runs, due to a variation in the energy V_0 of the particles responsible for the ionization, a fifth experimental check can be obtained by using the observed frequency, n_0, and $\tilde{n}_e$ in equation (23) to calculate the effective ionization-rate parameter

$$\langle \sigma v \rangle_{ne} = \frac{2 \pi \nu_{obs}}{\sqrt{\tilde{n}_e n_0}} \qquad (\eta \approx 1.0) \tag{29}$$

This quantity may then be plotted against the observed particle energy V_0 to determine whether this curve resembles in geometrical shape those tabulated for the gas in question. The use of experimental data to show a variation of effective cross section with particle energy implies that a suitable average can be defined for this quantity, if it varies over a cycle of oscillation. If such a variation in $\langle \sigma v \rangle_{ne}$ does occur over a cycle of oscillation (as opposed to a variation of $\langle \sigma v \rangle_{ne}$ for different experimental conditions), the small-amplitude analysis may not yield valid predictions.

A sixth experimental check of the theory can be obtained by looking for the effects of $G(\eta)$ and $H(\eta)$ on the relation between observed oscillation frequency and the product $\tilde{n}_e n_0$. Equation (28) states that the parameter η is inversely proportional to the

square of the observed oscillation frequency; low frequencies will be generally associated with large values of η, while high frequencies will be associated with low values of η. For low frequencies, therefore, η will tend to fall in the range $\eta \geq 1.0$, and equation (21) will be appropriate for the functional dependence of the frequency. An examination of equation (21) and of figure 3(b) for $H(\eta)$ as a function of η suggests that if the oscillation frequency is sufficiently low, a log-log plot of observed frequency as a function of the product will fall above an extension of a straight line with slope 1/2, appropriate to the square-root dependence alone. The expected behavior of such a data plot is shown schematically in figure 4.
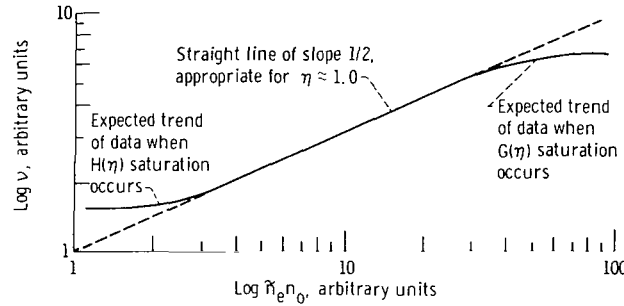
Figure 4. - Schematic log-log plot of observed frequency of oscillation as function of product of average electron and neutral number densities.

When the observed frequencies are high and η lies in the range $2/3 \leq \eta \leq 1.0$, equation (17) is the appropriate expression for the frequency. An examination of figure 3(a) shows that over this range $G(\eta) \leq 1.0$. A log-log plot of observed frequency as a function of the product $\tilde{n}_e n_o$ can therefore be expected to fall below the straight line of slope 1/2 at sufficiently high frequencies. This behavior is also shown schematically in figure 4.

In an experimental situation, the falloff due to the $G(\eta)$ dependence must be distinguished from a phenomenon which may be called "transit-time saturation." This phenomenon arises from the diffusion term in the continuity equations becoming important in the operation of the discharge and has the same qualitative effect on the data as the $G(\eta)$ term. Transit-time saturation and the spatially dependent diffusion term become important when the period of oscillation becomes comparable with the length of time required for a neutral molecule of average velocity v_o to traverse a characteristic radius of the discharge R. Therefore, transit-time saturation should occur, and the frequency should approach a constant value, when the discharge frequency is

$$\nu \sim \frac{v_o}{R} \text{ Hz} \tag{30}$$

If it is assumed that the neutral molecules have velocities appropriate to laboratory-room temperature and that the discharge has a characteristic radius of 5 centimeters, the transit-time saturation frequency is approximately 28 kilohertz for deuterium and helium and 12 kilohertz for neon gas in the present experimental apparatus.

The effect of $G(\eta)$ on the experimental data can be distinguished from transit-time saturation in two ways. First, when transit-time saturation occurs, the discharge should no longer be seen to oscillate in unison, with a single phase. A wave of ionization propagating in the discharge should be observable. A saturation due to $G(\eta)$ would not have this effect. A second method of distinguishing the two types of saturation is possible because the saturation frequency given by equation (30) is not a function of electron number density, while η, and hence $G(\eta)$, does depend on $\tilde{n}_e$ in the manner given by by equation (12).

These six experimental checks of the theoretical model are all qualitative in nature. A seventh and final check can be obtained by making an absolute measurement of the charged-particle and neutral number density along with the charged-particle energy, and then substituting $\tilde{n}_e$, n_o, and $\langle \sigma v \rangle_{ne}$ into equation (23) for a qualitative check against the observed frequency of oscillation. The obtaining of a reliable quantitative check is made difficult by the paucity of reliable data on the ionization-rate parameter $\langle \sigma v \rangle_{ne}$, in addition to the more usual experimental difficulties. Experimental values of this quantity are available for electron-neutral ionization of a few gases (refs. 12 and 13). Most of the ionization-rate coefficients are based on empirical curve fits (refs. 12 and 13), and are, in general, lower limits to the true value (ref. 13). Very little data of any kind are available on the ionization-rate coefficient for ion-neutral ionization processes.

EXPERIMENTAL INVESTIGATION

Experimental Apparatus

The superconducting magnet facility used in the experimental investigation has been described elsewhere (ref. 14). It consists of a magnetic mirror configuration with a 2.5 to 1 mirror ratio located in a 0.89-meter-diameter, 1.83-meter-long vacuum tank. The maximum magnetic field could be varied from 0.2 to 2.0 tesla during the course of the experiments. Unless noted otherwise, all data were taken at a maximum magnetic field of 1.0 tesla. The two magnetic field coils had an inside diameter of 18 centimeters and produced an axisymmetric magnetic field.

The operation and characteristics of the discharge used as the subject of the present investigation have been discussed in part elsewhere (refs. 2, 15, and 16). Of relevance

to the present discussion is the fact that the ions leaving the discharge are quite energetic, from 100 to 4000 electron volts per ion, while the electrons are less energetic, typically about 100 electron volts. In figure 5 is shown an isometric cutaway drawing of the superconducting coils with the discharge in operation. In figure 6 is shown a scaled cross-sectional view of the discharge, coils, and vacuum tank, looking down from the top. The positions of the collimated photomultiplier and the retarding-potential electrostatic energy analyzer are shown as they were during the experimental runs.

Figure 7 is a schematic drawing showing the diagnostic equipment used to measure the relevant experimental quantities. The neutral gas pressure in the vacuum tank was measured with an ion gage. It was assumed that the fluctuations in light intensity from the discharge were synchronous with fluctuations in the electron number density. This synchronism was verified by observing that the frequency of the light fluctuations was synchronous with the fluctuations of floating potential on a Langmuir probe inserted in the plasma, and also with fluctuations in the current collected by the electrostatic energy analyzer. The fluctuations in light output from the discharge were monitored by a collimated type IP-28 photomultiplier. The output of this photomultiplier was fed into a Nelson-Ross Inc. model 001 spectrum analyzer for frequencies below 20 kilohertz and to a Nelson-Ross model 012 spectrum analyzer for frequencies in the range of 20 to
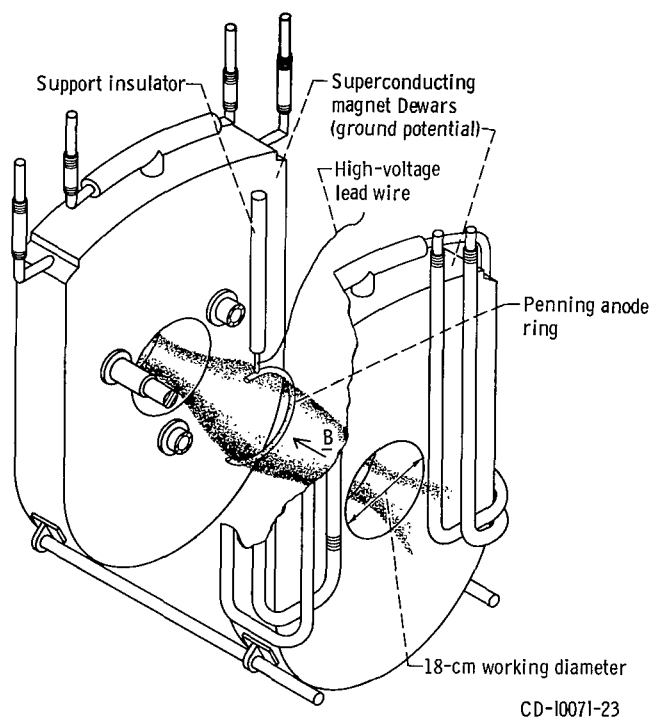

Figure 5. - Isometric cutaway drawing of modified Penning discharge and magnetic field coils. Maximum midplane diameter of discharge, 16 centimeters.
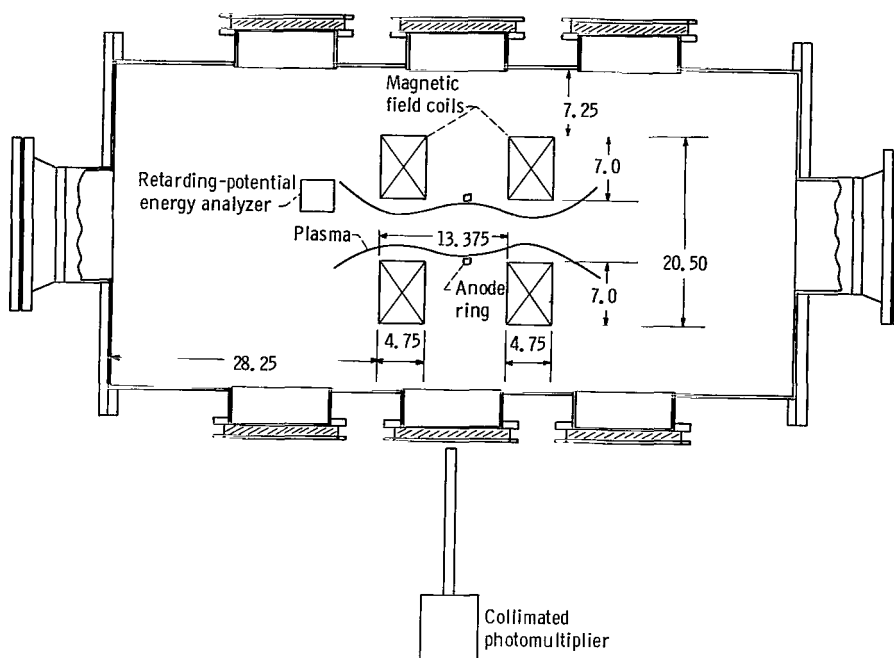
Figure 6. - Cutaway top view of apparatus showing placement of collimated photomultiplier, retarding-potential energy analyzer, and anode ring. Vacuum tank is 0.89 meter in diameter and 1.83 meters long. Dimensions are in centimeters.
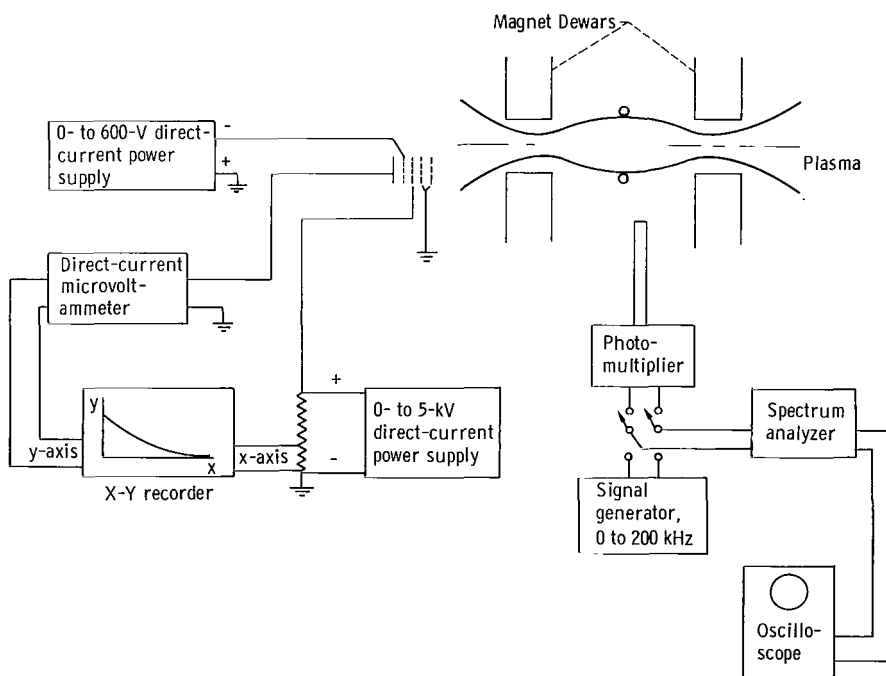

Figure 7. - Schematic drawing of principal experimental equipment for electrostatic ion energy analyzer and measurement of frequency of fluctuations in light output.

100 kilohertz. The output of the spectrum analyzer used was then displayed on an oscilloscope.

The retarding potential for the electrostatic energy analyzer was provided by a well-filtered 5-kilovolt direct-current power supply. The collector current from the analyzer was fed into an electronic microvolt-ammeter. The output of this instrument was then used to drive the y-axis of an X-Y recorder. The retarding potential provided by the 5-kilovolt power supply was monitored by a precision voltage divider and was used to drive the x-axis of the X-Y recorder.

Experimental Procedure

The frequency of oscillation was measured by monitoring the light output from the plasma with a collimated photomultiplier and then displaying the fundamental frequency of the fluctuations in light output on a spectrum analyzer. Harmonics of the fundamental frequency were usually visible on the oscilloscope display, due to the nonsinusoidal nature of the waveform of $n_e(t)$. The fundamental frequency of the fluctuations in light output was identified by alternately displaying this frequency and the frequency of the output of a signal generator, as shown in figure 7. The frequency of the signal generator was adjusted until the two peaks were seen to coincide on the spectrum analyzer. The oscillation frequency was then read off the dial of the signal generator.

The presence in the discharge plasma of oscillations, hot ions, and a magnetic field made it very undesirable to rely on Langmuir probes for a measurement of the electron number density. In addition, the plasma energy density was sufficiently high to destroy the probes under many conditions of operation. Relative measurements of the electron number density were made by noting the initial current and ion kinetic temperature obtained by analysis of the retarding-potential curve from an electrostatic energy analyzer. The characteristics and operation of the electrostatic energy analyzer used in these investigations are discussed in reference 16. As indicated in figure 7, an integrated ion energy spectrum can be formed on an X-Y plotter by graphing the current flowing to the collector as a function of the voltage applied to the retarding grid. As explained in reference 16, these integrated energy spectra can be analyzed by a computer program to produce (among other data) the kinetic temperature of the ions V_o, the initial current I_1, and the half-angle in velocity space of the escape cone θ_o. This initial current is given by

$$I_1 = \frac{\tilde{n}_e e v_i A}{2\pi^{1/2}} \sin^2\theta_o G_o \tag{31}$$

where $\tilde{n}_e$ is the average charged-particle density in the discharge, v_i is the ion velocity, and A is the area of the energy analyzer aperture. The parameter G_O is a geometry factor accounting for the inhomogeneity of the discharge, the dispersal of the plasma as it travels from the discharge to the energy analyzer, and the transmissivity of the analyzer itself. This geometry factor was constant for all experimental runs and is of the order of 10^{-6} in the present experiment, based on a checkpoint obtained with Langmuir probes.

In figure 8 is shown a typical integrated energy spectrum from the X-Y recorder. Also shown in this figure is the best-fitting curve as determined by the computer program, with the best-fitting values of I_1, V_O, θ_O, and "plasma potential" V_1 as indicated. A relative measure of the average charge density in the discharge can be obtained by writing equation (31) in terms of the parameters I_1, θ_O, and V_O

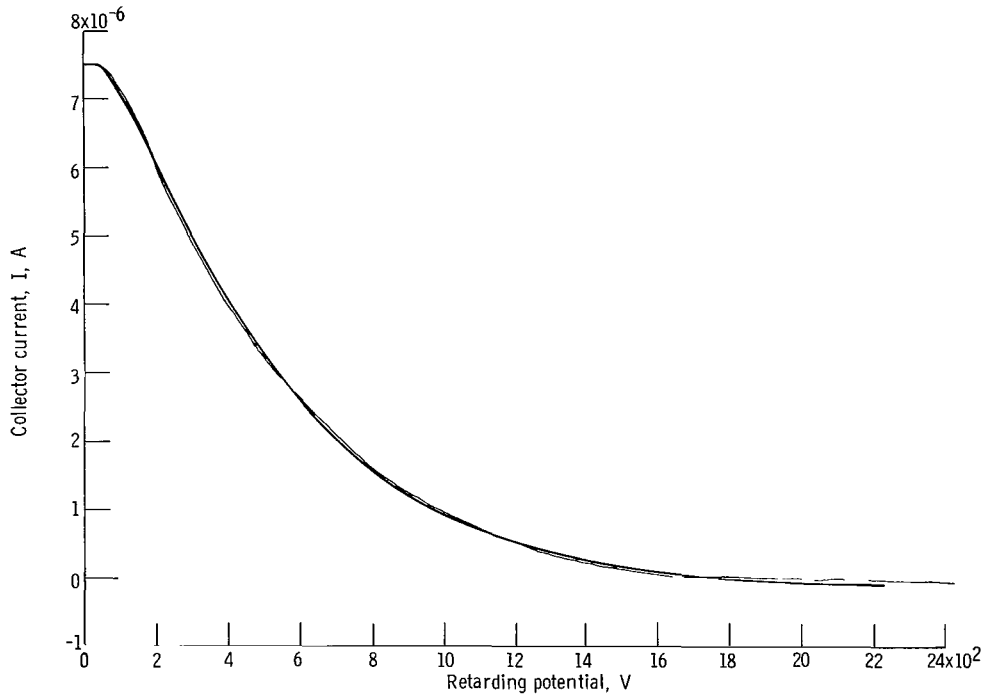$$n_e \approx G_O^{-1} \frac{I_1}{V_O^{1/2} \sin^2 \theta_O}$$ (32)

Figure 8. - Retarding-potential curve showing theoretical curve with best-fitting initial current and ion kinetic temperature. Initial current, 7.64×10^{-6} ampere; $I_0 = -0.14 \times 10^{-6}$ ampere, kinetic temperature of ions, 347 electron volts; potential at which plasma is floating, 40 volts; half-angle in velocity space of escape cone, 39°; mean square error, 0.44 percent.

where it is assumed that G_0 is constant for a particular gas and for a fixed geometrical relation between the analyzer and the discharge.

The neutral-particle density in the vacuum tank was measured by the ion gage mentioned in the previous section. This measured pressure was converted to absolute pressure by gage factors obtained by comparing the ion-gage reading with that of an extremely sensitive diaphragm-type pressure meter, whose deflections were sensed and amplified electronically.

A large majority of the experimental runs were devoted to checking out the square-root dependence of the frequency on the product $\tilde{n}_e n_0$. For a given gas (deuterium, neon, and helium were used), about a dozen series of runs were taken, each series at a different neutral background pressure. The runs within each series were taken at different anode voltages, which caused the electron density in the discharge to vary from one run to the next. An X-Y recording was made of the retarding-potential curve from the electrostatic energy analyzer during each run, and the frequency of oscillation was measured simultaneously by the superposition method described previously. The maximum magnetic field was held constant at 1.0 tesla during these runs.

Several series of runs were made to measure the peak-to-peak amplitude of oscillation as a function of η. The magnetic field was fixed at $B_{max} = 1.0$ tesla, and the oscillation frequency and the anode current were measured as the anode voltage was varied. The peak-to-peak amplitude was measured by recording the amplitude of the fundamental frequency of oscillation as displayed on the spectrum analyzer.

Several series of runs also were made to determine whether the frequency was a function of the magnetic field. In this case, the anode voltage was fixed for a given series, and the frequency and retarding-potential curves were measured as functions of the magnetic field strength. Because small variations occurred in the neutral and electron number densities during a series (it took about 4 hr to vary B_{max} over its range $0.2 \leq B_{max} \leq 2.0$ T), the frequency coefficient

$$\nu_0 \equiv \frac{\nu_{obs}}{\sqrt{\tilde{n}_e n_0}} = \frac{\langle \sigma v \rangle \, n_e}{2\pi} \tag{33}$$

was plotted against magnetic field.

Range of Experimental Parameters

The approximate range of the experimental parameters appropriate to this experiment are listed in table I. The upper and lower limits quoted for the electron number density are very uncertain and may be off by a factor of 5. As will be shown, how-

22

TABLE I. - RANGE OF EXPERIMENTAL PARAMETERS

Characteristic	Low value	Typical value	High value
Background pressure, torr	5×10^{-7}	10^{-5}	10^{-4}
Approximate electron density, electrons/cm^3	10^6	10^8	5×10^9
Electron kinetic temperature, eV	10	100	400
Ion kinetic temperature, eV	100	700	4000
Maximum magnetic field, T	0.2	1.0	2.0
Oscillation frequency, Hz	100	5000	8×10^4
Debye length (100-eV electrons), cm	0.10	0.75	7.5
Neutral-neutral mean free path collision (D_2), m	1.03	10.3	206

ever, <u>relative</u> measurements of electron density could be made to within 25 percent. The upper and lower limits of the range quoted for the electron kinetic temperature may be incorrect by a factor of 2. The presence of the energetic ions made absolute deter- mination of the electron density and temperature very difficult in this experiment.

The Debye length at the extreme lower end of the density range was comparable to the dimensions of the discharge. However, most of the data were taken when the Debye distance was less than 1 centimeter. Since there was no apparent qualitative change in the character of the data as the Debye distance varied over its range, all data were treated as if the assumption of quasi-neutrality were satisfied. Of the gases studied, deuterium gas has the shortest neutral-neutral mean free path. These mean free paths are much longer than the discharge dimensions, a significant difference from the situa- tion existing in classical gaseous discharge tubes.

Analysis of Experimental Error

Error bars are not drawn on the data points displayed graphically in the following sections. Instead, some general remarks are made regarding the limits of error ap- propriate to various ranges of the measured parameters.

The oscillator used as a frequency standard during this series of experiments was initially checked against a 1-megahertz counter with an oven-controlled crystal fre- quency standard. It was found that the reading on the dial of the oscillator was within 1 percent of the reading on the counter over the frequency range 10^2 to 10^5 hertz. The

principal error in measuring the frequency was not inaccuracy of the standard used, but uncertainty introduced by short-term drifts of the electronics of the spectrum analyzers (under high dispersion), broadness of the frequency peaks with resulting difficulty of defining the true maximum, poor signal-to-noise ratio, and drift of the discharge operating conditions during a run. It is estimated that the resulting total error in frequency was no more than that shown in table II for the frequency ranges shown.

TABLE II. - EXPERIMENTAL

ERRORS OF FREQUENCY

MEASUREMENT

Frequency range, Hz	Total error, percent
100 to 400	20
400 to 1000	3
1000 to 10^4	5
10^4 to 10^5	2

The error in relative measurements of the neutral number density in the vacuum tank was no more than 5 percent. The magnetic field was measured by a rotating-coil gaussmeter rated at 1 percent accuracy.

The errors that can arise in measuring the parameters I_1, θ_o, and V_o contained in equation (32) are discussed in reference 16. It was shown in this reference that I_1 could vary by as much as 14 percent for supposedly identical runs and that V_o could vary by as much as 6 percent. Considering that runs were taken with a given gas over periods as long as three weeks, it appears reasonable to estimate an error of 20 percent in relative measurements of the electron number density. The total error in relative measurements of the product $\tilde{n}_e n_o$ is therefore 25 percent. This is a rather large error, but an attempt was made to compensate for it in the present experiment by taking a large number of data points, which thus improved the statistics, and by taking data over a wide range of the product $\tilde{n}_e n_o$, which amounted to nearly 6 orders of magnitude in the present experiment.

In presenting the experimental results, it was convenient to assume that the ionization-rate parameter $\langle \sigma v \rangle_{ne}$ was constant for every run taken with a particular gas and then to plot the observed frequency as a function of the product $\tilde{n}_e n_o$. In a significant minority of cases, the error limits discussed above for ν and $\tilde{n}_e n_o$ do not overlap the best-fitting line through all the data points. This failure to overlap may be

attributed to the variation of the electron kinetic temperature from run to run, which then caused $\langle\sigma v\rangle_{ne}$ to vary significantly.

Of the runs taken in the laboratory, approximately 5 percent of those taken with deuterium and helium gas were discarded. These runs were discarded because of a bad fit of the theoretical to the actual retarding-potential curve (usually implying a very non-Maxwellian velocity distribution), drift of tank pressure or another parameter during an experimental run, contamination of the gas by outgassing or leakage into the vacuum tank, or difficulty in distinguishing the oscillation peaks from noise on the spectrum analyzer display. An additional 15 percent of the neon data points (about 20 percent altogether) were discarded because they were beyond the $G(\eta)$ saturation "knee." This phenomenon is described in the section EXPERIMENTAL RESULTS below.

The parameter ν_o given by equation (33) has error limits of about ±15 percent, which follows from the 25 percent error limits assigned to the product $\tilde{n}_e n_o$ and the error limit assigned to the measured frequency in table II. The parameter ν_o may also vary if there is a significant variation in the energy of the particles responsible for ionizing the neutrals, and hence in $\langle\sigma v\rangle$.

EXPERIMENTAL RESULTS

Results with Deuterium Gas

Two hundred and forty-seven experimental runs with deuterium gas were of usable quality. Each of these runs included an integrated energy spectrum of the ions in the form of a retarding-potential curve, a measurement of the background neutral gas pressure in the vacuum tank, and a measurement of the oscillation frequency as determined from the frequency of the fluctuations in light output.

The observed frequency is plotted as a function of the product $\tilde{n}_e n_o$ (in arbitrary units) in figure 9 for the 247 data points taken with deuterium gas. If the predicted relation given by equation (23) holds for these data, and if the ionization-rate parameter $\langle\sigma v\rangle_{ne}$ is a constant, the data in the log-log plot of figure 9 should have a slope of 1/2. The data shown plotted in figure 9 were used as input to a logarithmic least-squares computer program that obtained a best fit to a curve of the form

$$\nu = \nu_o (\tilde{n}_e n_o)^E \tag{34}$$

A best-fitting curve was obtained in which both ν_o and E were left as free parameters, and this yielded

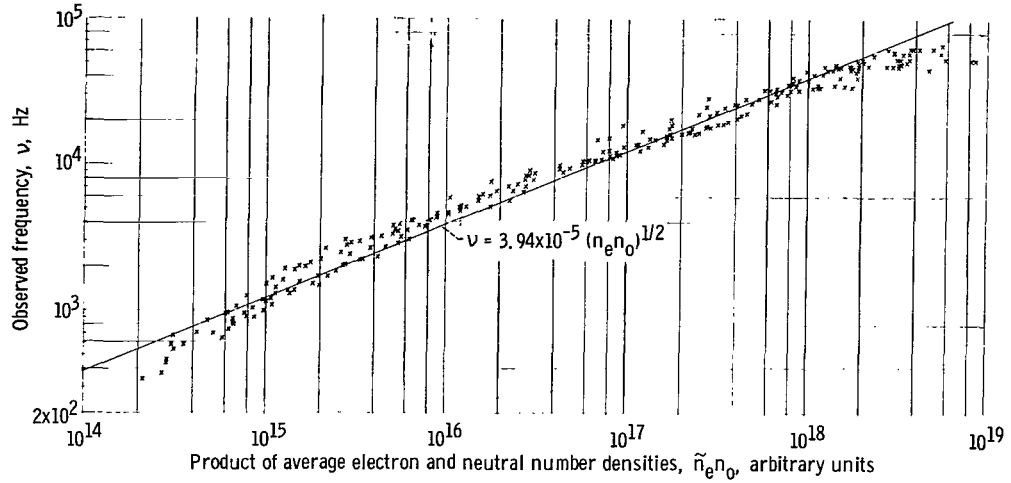$$\nu = 5.4812\times10^{-5}(\tilde{n}_e n_o)^{0.49134} \tag{35}$$

Figure 9. - Log-log plot of observed frequency of oscillation in deuterium gas as function of product of charged-particle and neutral number density. Best-fitting line, of slope $\frac{1}{2}(\nu \sim \sqrt{\tilde{n}_e n_0})$, is drawn through data.

The slope of this line is quite close to the theoretically predicted value of $1/2$. When a best fit was obtained for the slope $E = 1/2$, the best-fitting curve was given by

$$\nu = 3.9434 \times 10^{-5} \left(\tilde{n}_e n_0\right)^{1/2} \qquad (36)$$

This best-fitting straight line of slope $1/2$ has been drawn through the data presented in figure 9.

An examination of the data in figure 9 reveals no tendency of the data points to fall above the straight line at low frequencies, due to $H(\eta)$ saturation. There is, however, a noticeable tendency of the data to fall below the straight line at the highest frequencies. The knee of this saturation was taken as $\tilde{n}_e n_0 = 2.0 \times 10^{18}$, and all data points above this value of $\tilde{n}_e n_0$ were accordingly excluded from the curve-fitting process that resulted in equations (35) and (36). The raw data for each of the several run series showed that the frequency of the knee in figure 9 was not a function of the electron number density. Two collimated photomultipliers were placed at different axial stations, and propagating waves were observed in the axial direction. On the basis of this evidence, it is probable that the saturation shown in figure 9 is transit-time saturation, rather than the electron-number-density-dependent $G(\eta)$ saturation.

Several series of runs were taken in which the frequency was measured as a function of magnetic field strength. The quantity ν_0, given by equation (33), is shown plotted as a function of magnetic field for two series of runs in figures 10(a) and (b). After the changes of $\tilde{n}_e$ and n_0 during the time required to vary the magnetic field have been compensated for by using the parameter ν_0, it is evident that the frequency is independ-
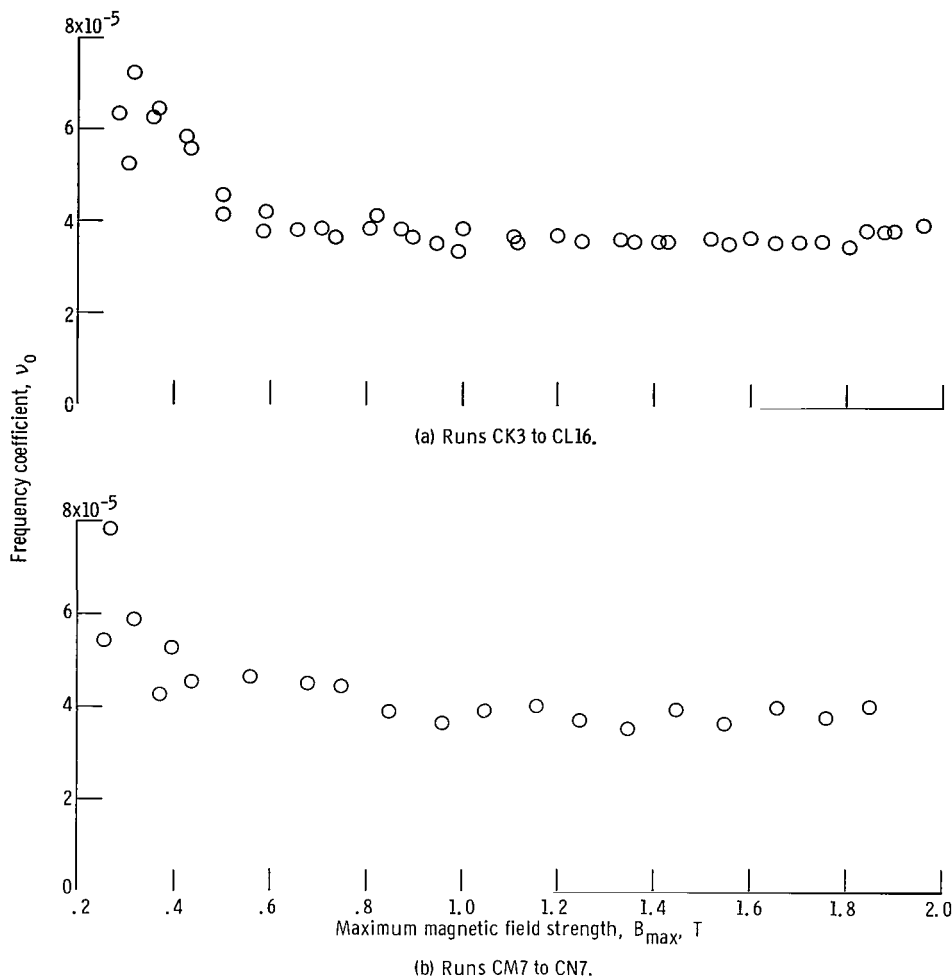
(a) Runs CK3 to CL16.

(b) Runs CM7 to CN7.

Figure 10. - Plot of frequency coefficient for deuterium gas as function of maximum magnetic field.

ent of magnetic field over more than a factor of 4 in magnetic field strength. Most of the variation shown in figure 10 is within the 15 percent error limits assigned to the quantity ν_0.

Results with Neon Gas

Three hundred and thirty-seven individual runs with neon as the working gas are plotted in figure 11. A best fit was obtained to equation (34) for these 337 runs, with the following result

$$\nu = 3.0147 \times 10^{-4} (\tilde{n}_e n_0)^{0.50112} \tag{37}$$

27
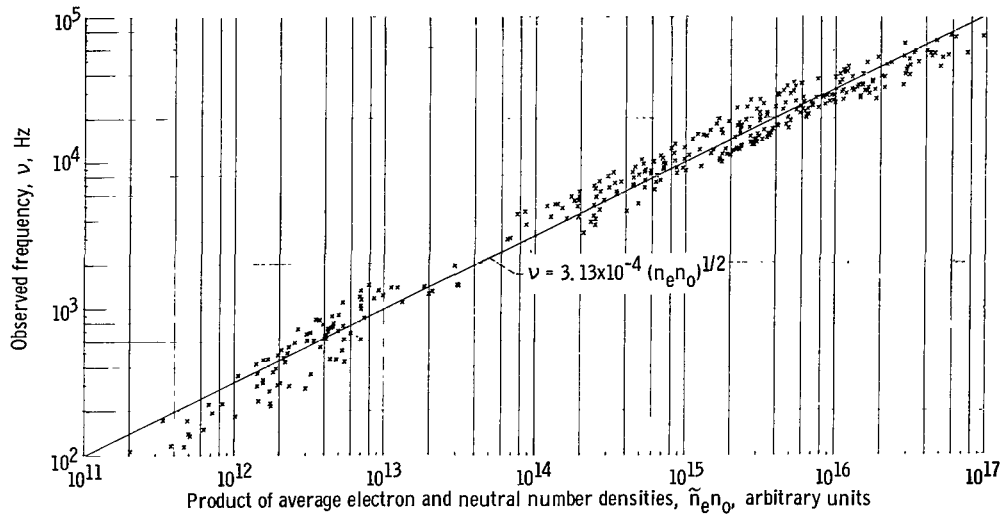
Figure 11. - Observed frequency as function of product of average electron and neutral number densities for neon gas. Best-fitting line of slope 1/2 is drawn through data.

The best-fitting slope is quite close to the theoretically predicted value of 1/2. The best-fitting relation with slope equal to 1/2 is given by

$$\nu = 3.1313 \times 10^{-4} (\tilde{n}_e n_0)^{1/2} \tag{38}$$

A run series, taken at a single constant background pressure of neutral gas, is shown plotted in figure 12 along with the best-fitting straight line (given by eq. (38)) of slope 1/2 for the entire set of data. These data show a saturation at high frequency.
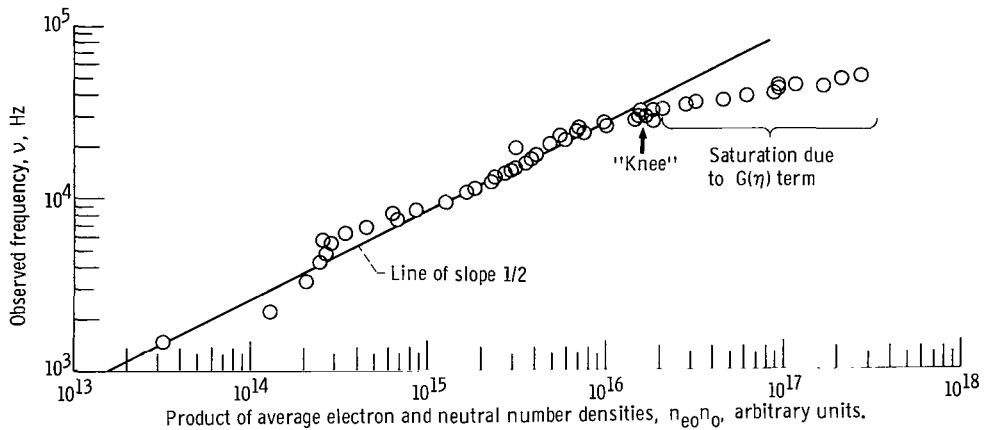
Figure 12. - Runs CY 2 to CZ 25 taken with neon gas at single neutral background pressure. Saturation is probably due to $G(\eta)$ term, since frequency of knee varied with electron number density. Data lying beyond knee were not included among points plotted in figure 11.

Comparison with other series of runs showed that the frequency of the knee was a function of the electron number density. In addition, no propagating waves were observed in the vicinity of these knees with a pair of collimated photomultipliers. It therefore appears probable that this saturation phenomenon in neon gas is due to $G(\eta)$ saturation rather than transit-time saturation. Since the data beyond the knees of these neon runs would have seriously affected the curve fits to the data below the knees, the data above the knees were not included in the 337 data points which were plotted in figure 11, and which formed the basis for the curve fits of equations (37) and (38).

A series of runs was taken to measure the effect of magnetic field on the frequency of oscillation for neon gas. The quantity ν_O given by equation (33) is graphed as a function of magnetic field strength in figures 13(a) and (b). It was found that the quantity
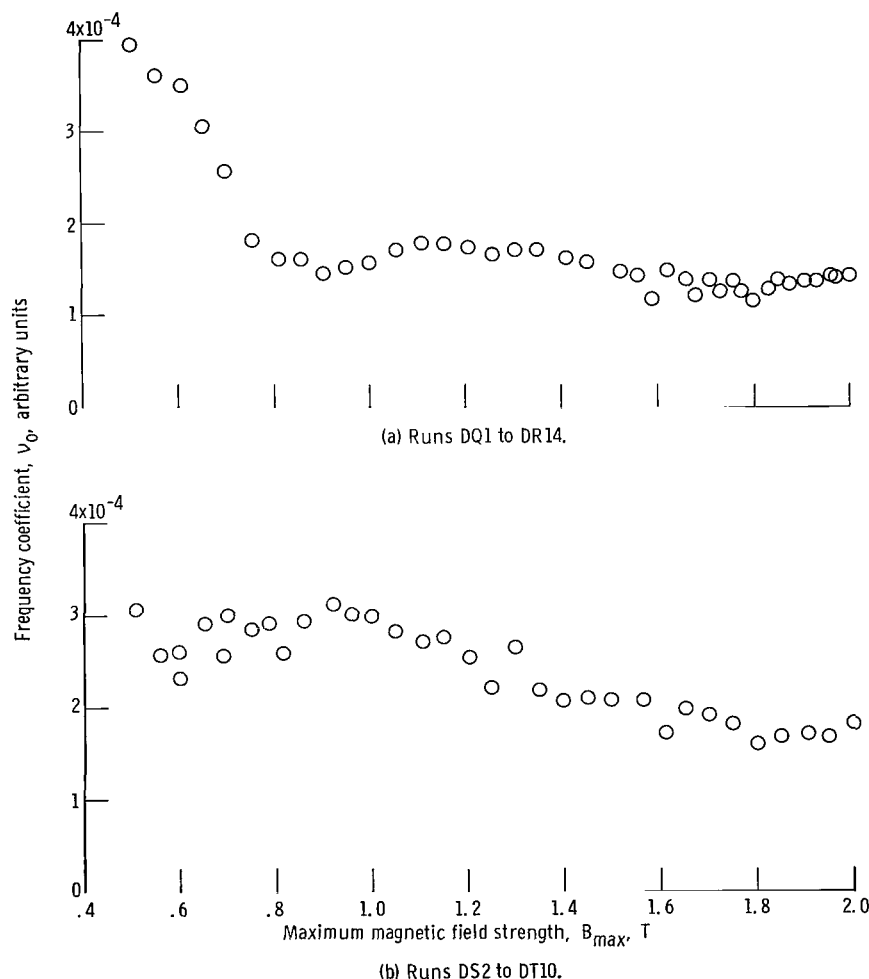

(a) Runs DQ1 to DR14.

(b) Runs DS2 to DT10.

Figure 13. – Frequency coefficient for neon gas as function of maximum magnetic field.

ν is virtually independent of magnetic **field over more than** a factor of 3 in magnetic field strength. Most of the variation shown lies within the 15 percent error limits assigned to the frequency coefficient ν_o.

Results with Helium Gas

In the two sets of runs with deuterium and neon gas it was assumed that the ionization-rate coefficient $\langle\sigma v\rangle_{ne}$ was constant throughout the experiment. The slopes of the best-fitting straight lines were sufficiently close to the theoretically predicted value of 1/2 that this assumption appears to be borne out, transit time and $G(\eta)$ saturation excepted. In the runs with helium gas, however, $\langle\sigma v\rangle$ does not appear to be constant during the experiment.

Three hundred and ninety-one runs were taken with helium gas. The observed values of $\tilde{n}_e n_o$ and oscillation frequency are plotted in figure 14. The data are much more widely spread than with the other two gases and do not cluster along a straight line on this log-log plot. The best-fitting straight line through these data is given by

$$\nu = 6.5292\times10^{-7}(\tilde{n}_e n_o)^{0.60528} \tag{39}$$

The slope is sufficiently far from the value of 1/2 predicted theoretically that there is a possibility that variations in $\langle\sigma v\rangle$ occurred during the helium runs. It was assumed that the parameter ν_o defined by equation (33) was proportional to the ionization-rate coefficient for ions $\langle\sigma v\rangle_{ni}$ since the maximum rate coefficient for ionization by ions is
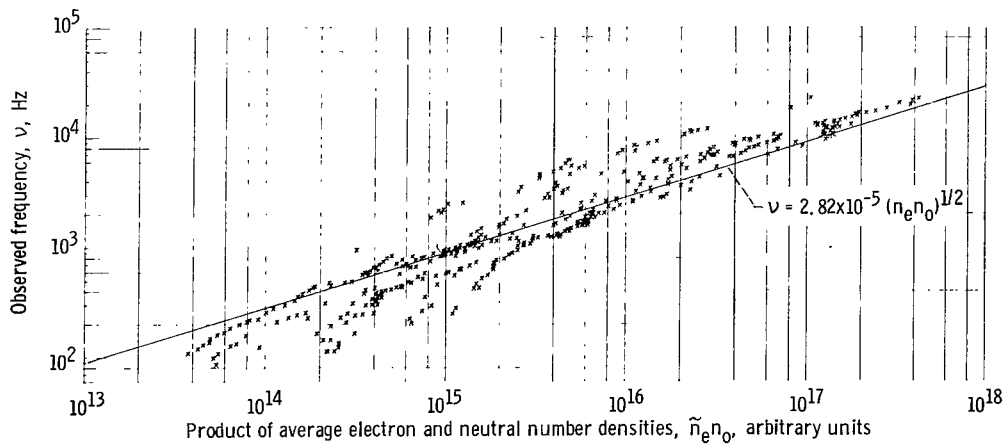

Figure 14. - Observed frequency as function of $\tilde{n}_e n_o$ for helium gas. Best fitting line of slope 1/2 is drawn through data.
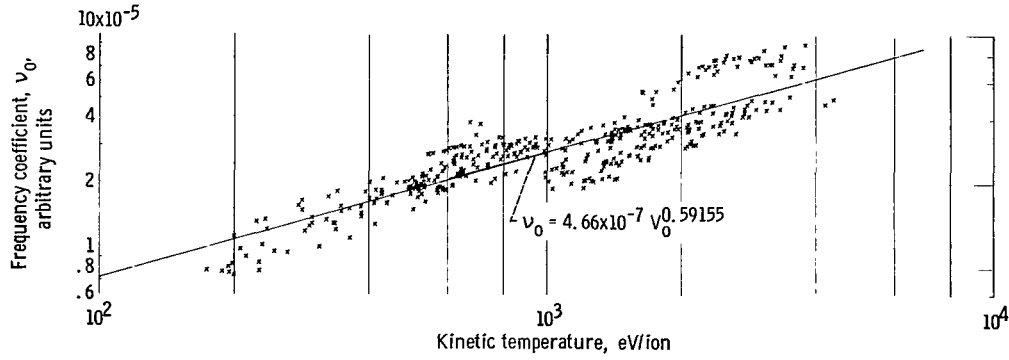
Figure 15. - Frequency coefficient as function of ion kinetic temperature for helium. Best-fitting line, given by equation (40), is drawn through data.

greater than that for electrons in helium. A graph of ν_0 as a function of the ion kinetic temperature V_0 is presented for the 391 helium runs in figure 15. These data cluster roughly around a straight line on this log-log plot, the best-fitting value of which has the form

$$\nu_0 = 4.6572\times10^{-7}\, V_0^{0.59155} \tag{40}$$

This relation implies that $\langle\sigma v\rangle_{ni}$ is a monotonically increasing function of ion energy for values of V_0 up to 4 kiloelectron volts per ion. This, in turn, suggests that the ionization process active in helium in this discharge is ion-neutral impact ionization. No cross sections or ionization rate coefficients appear to be available for the process

$$He^+ + He \to 2He^+ + e$$
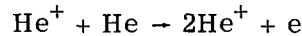
other than those cited in references 17 and 18. These suggest that the above reaction has a maximum above 3.2 kiloelectron volts per ion, and is therefore consistent with this interpretation.

Equation (40) was used as an empirical relation between ν_0 and V_0 to calculate a reduced frequency

$$\nu_r \equiv \nu_{obs}\left(\frac{1000}{V_0}\right)^{0.59155} \tag{41}$$

where ν_{obs} is the observed oscillation frequency. The reduced frequency ν_r may be thought of as the frequency that would have been observed if the helium ions all had a
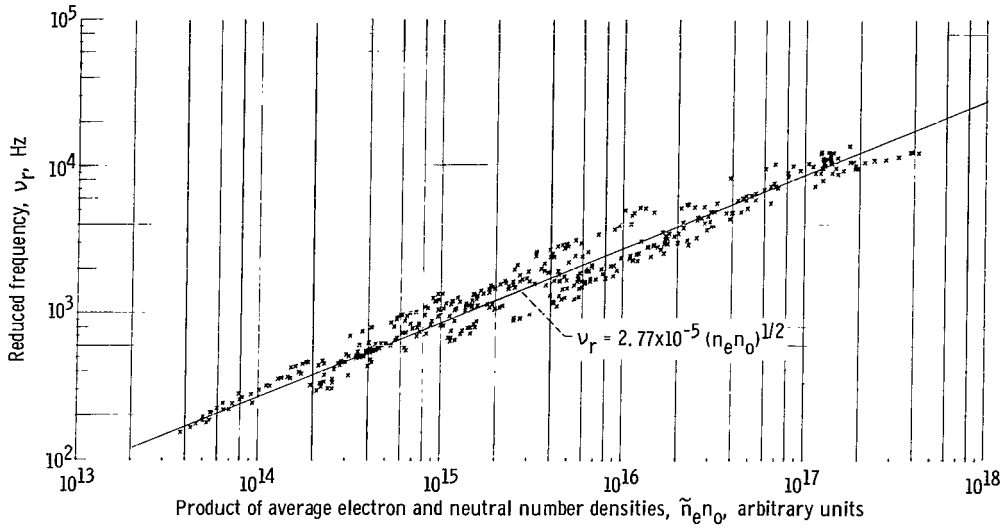
31

Figure 16. - Reduced frequency, given by equation (41), for helium data as function of product of average electron and neutral number densities. Best-fitting line of slope 1/2 is drawn through data. Reduced frequency is frequency that would have been observed if ions had kinetic temperature of 1 kilovolt per ion.

kinetic temperature of 1.0 kiloelectron volt per ion. The reduced frequency ν_r is plotted as a function of the product $\tilde{n}_e n_o$ in figure 16 along with the best-fitting line of slope 1/2. The points in figure 16 are much more closely clustered about the line of slope 1/2 than are those of figure 14 about the best-fitting straight line given by equation (39). This improvement in the ordering of the data implies that the observations are consistent with the continuity-equation oscillation mechanism after the energy variation of $\langle \sigma v \rangle_{ni}$ is accounted for. While the helium data cannot be used to demonstrate agreement with the predictions of the mathematical model, it has been shown that these data are consistent with it.

In figures 17(a) and (b) the parameter ν_o is plotted as a function of the magnetic field for a run taken with helium gas. It was found that the frequency coefficient ν_o is approximately independent of magnetic field strength over more than a factor of 2 in magnetic field. Much of the variation in ν_o shown in figure 17 falls within the 15 percent error limits assigned to ν_o. The residual variation of ν_o is greater than was the case with deuterium or neon gas, and this is probably due to the variation in $\langle \sigma v \rangle_{ni}$ with ion energy as the magnetic field changed.

Before leaving the subject of helium gas, the author would like to point out a peculiar and unexplained relation that appeared in this gas, and in this gas only. In figure 18 is shown a plot of the observed frequency as a function of the charged-particle density $\tilde{n}_e$ for the helium data. The data lie quite close to a pair of best-
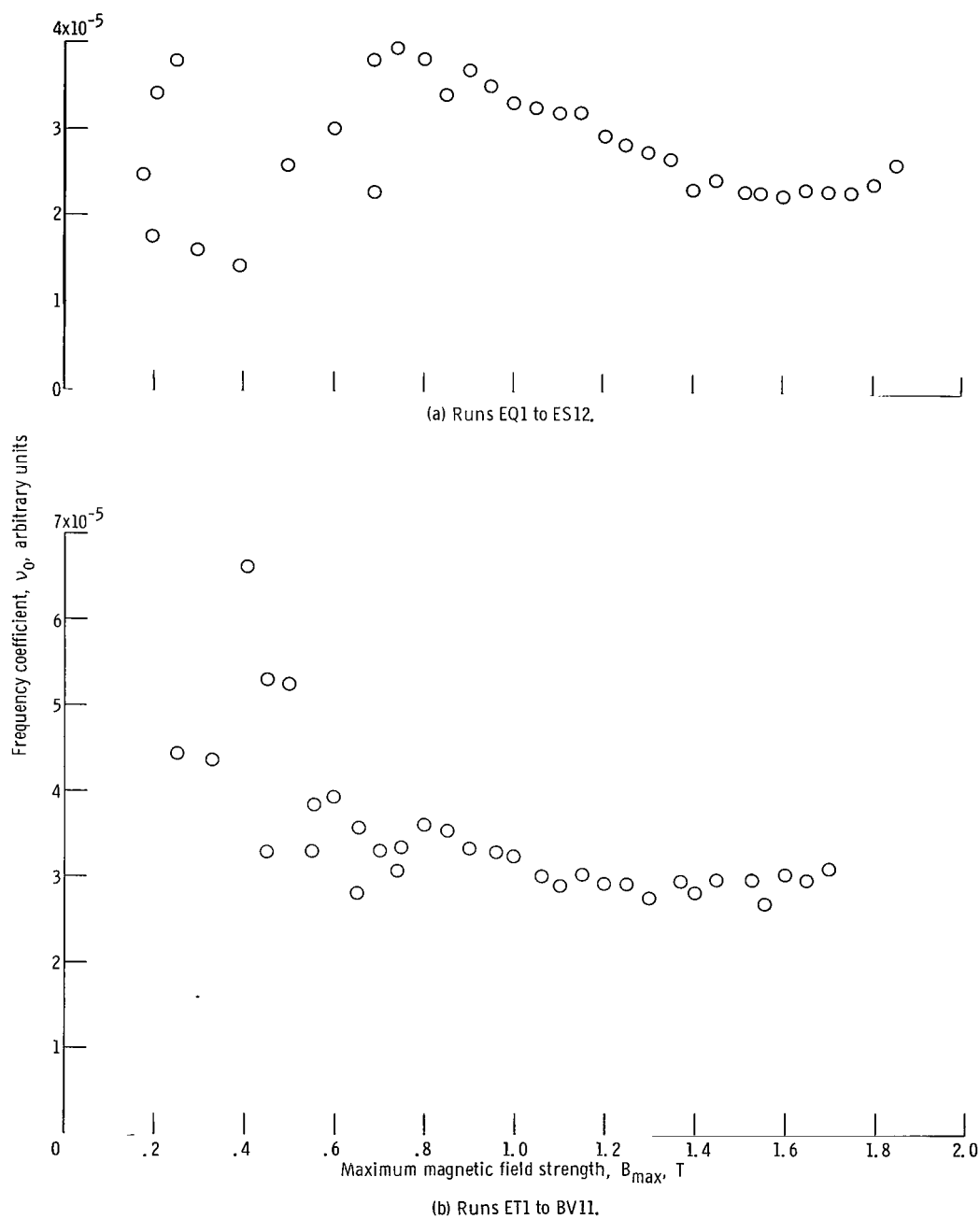
(a) Runs EQ1 to ES12.

(b) Runs ET1 to BV11.

Figure 17. – Frequency coefficient for helium gas plotted as function of maximum magnetic field.
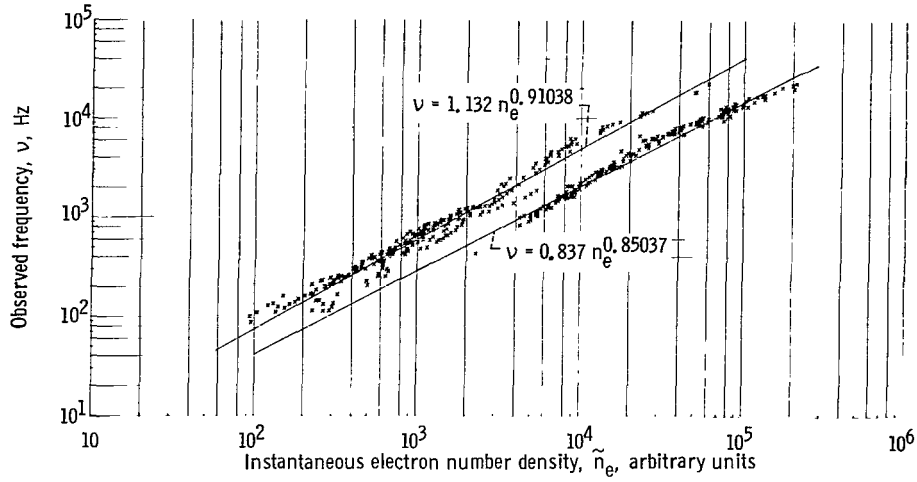
Figure 18. - Observed frequency for helium gas plotted as function of mean electron number density. Best-fitting lines given by equations (42) and (43) are drawn through these data. No explanation is known which accounts for this regularity in the data.

fitting straight lines on this log-log plot, the upper left of which is given by

$$\nu_{obs} = 1.1317 \, \tilde{n}_e^{\,0.91038} \tag{42}$$

and the lower right of which is given by

$$\nu_{obs} = 0.8368 \, \tilde{n}_e^{\,0.85037} \tag{43}$$

The fact that the data cluster around two straight lines rather than one is an artifact of the curve-fitting process for the retarding-potential curves from which the relative values of $\tilde{n}_e$ were calculated for helium gas. The upper left line given by equation (42) represents data that were definitely non-Maxwellian and whose best-fitting energy spectrum was appropriate to a distribution function with particles evenly spread between two limiting energies V_1 and V_2 (eV/ion), and with no angular spread in velocity space. This non-Maxwellian velocity distribution was not present in deuterium or neon gas.

The lower right curve represents data that best fit a Maxwellian velocity distribution, with a wide angular spread in velocity space. The retarding-potential curves from which the two classes of data in figure 18 were taken did not differ by as much as the separation of the two types of data seem to suggest. In actual fact, the ion energy distribution for helium gas was so non-Maxwellian that relatively small geometrical changes in the shape of the retarding-potential curves made the difference between one or the other giving the best fit.

34

The retarding-potential curves for helium revealed a generally much more non-Maxwellian velocity distribution than either deuterium or neon. Had the data for these latter two gases been plotted in the same manner as figure 18, the data for a given frequency would have been spread out over about two orders of magnitude in $\tilde{n}_e$ and would not have been clustered about a straight line.

The author does not have an explanation for the relation shown in figure 18, nor for the fact that it appeared only in helium gas. The theory for the continuity-equation instability does not predict a power-law dependence of oscillation frequency on $\tilde{n}_e$ with a slope of approximately 0.90, nor does the theory of any other plasma oscillation known to the author. It is tempting to dismiss the correlation revealed by figure 18 as a mere coincidence, a relation with no basis in physical theory. It is the belief of the author that a more profound understanding of the mechanisms operating in the discharge, including its energy balance, will reveal that equations (42) and (43) result from the dynamical characteristics of the discharge. The existence of the correlation represented by equations (42) and (43) is believed to be of some interest as a fact requiring explanation by a more complete theory of the discharge than the one presented herein.

Observations of Waveform and Amplitude

If the continuity-equation mechanism was responsible for the oscillations observed, the waveform should have the cuspoid shape illustrated by figure 2, when the average charged-particle density is either quite low or quite high and η is at the end of its range. In figures 19(a) to (d) are shown four typical waveforms of the light intensity from the discharge displayed on the oscilloscope as a function of time. Deuterium gas was used. These waveforms are definitely not sinusoidal and resemble the Jacobian elliptic function in their sharp maxima and their broad, flat minima. The waveforms do not resemble those of figure 2 in that their minima are offset from the zero level located at the bottom of the graticule.

The waveforms obtained at large and small values of η in the other gases investigated were qualitatively similar to those shown in figure 19. Figure 20 is a plot of light intensity and electron density as a function of time in a 2-torr closed gaseous discharge tube containing neon gas, as reported by Polman, et al., (ref. 19). This low-frequency oscillation (approx. 2 kHz) probably arises from the continuity-equation mechanism, and it is interesting to note the great similarity between figure 20 and the waveform displayed in figure 2(c).
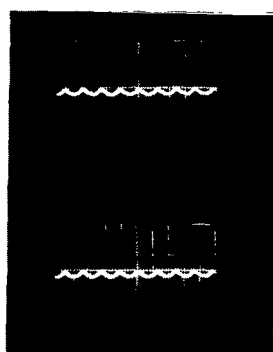
The peak amplitude of the fundamental frequency of oscillation was read off the display of a spectrum analyzer and plotted as a function of η in figure 21. The param-
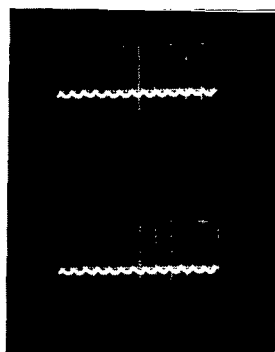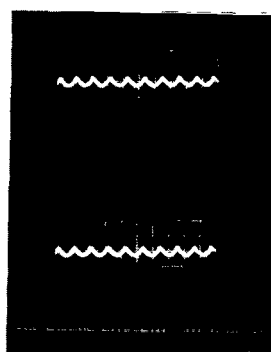
(a) Anode current, 4.0 milli-
amperes; 0.1 millisecond/
centimeter; 0.2 volt/inch.
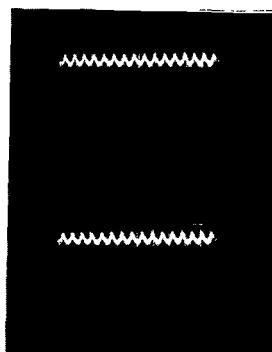
(b) Anode current, 6.0 milli-
amperes; 0.1 millisecond/
centimeter; 0.2 volt/inch.

(c) Anode current, 8.0 milli-
amperes; 0.5 millisecond/
centimeter; 0.5 volt/inch.

(d) Anode current, 10.0 milli-
amperes; 0.5 millisecond/
centimeter; 0.5 volt/inch.

Figure 19. - Light output as function of time. Maximum magnetic field,
1.0 tesla; pressure, 7.5×10^{-6} torr; deuterium gas. Zero at bottom of
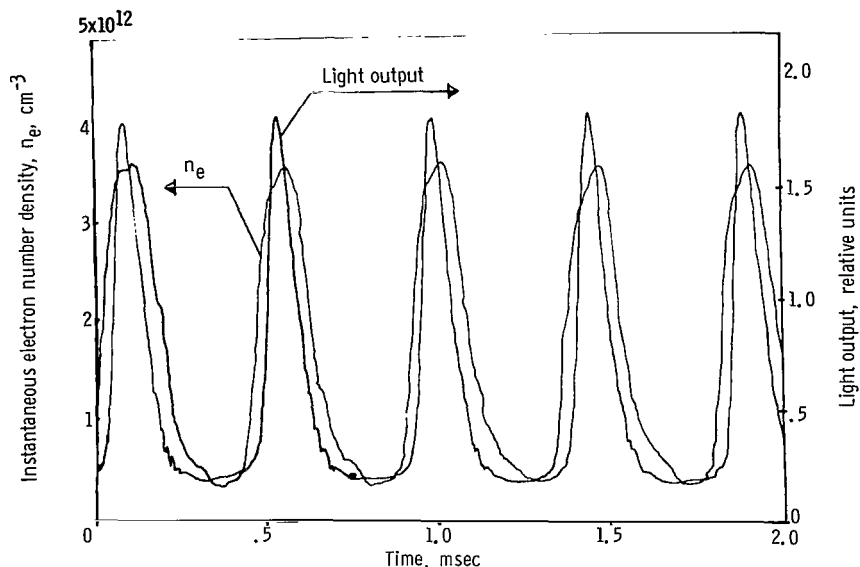graticule; time increases from right to left in all cases.

Figure 20. – Observed light output and electron number density as function of time in 2-torr neon discharge tube with current of 1 ampere. Note waveform characteristic of Jacobian elliptic functions (like fig. 2(c)). (Reproduced from Polman, et al., ref. 19.)

eter η was computed by using equation (28) and was then normalized to 1 for the value of η for which the amplitude of oscillation was a minimum. This procedure was necessary since it was not possible to make an absolute measurement of the ionization-rate parameter $\langle \sigma v \rangle_{ne}$ and thereby to establish directly the conditions for which $\eta = 1.0$. Figure 21 refers to deuterium gas, but qualitatively similar data were also taken with neon and helium gas.

The behavior of the peak-to-peak amplitude of oscillation with η is qualitatively that predicted by equations (24) and (25). The peak-to-peak amplitude is large for small η, decreases to a minimum value, then increases again as η goes to infinity. The observed oscillations below $\eta = 2/3$ arise from failure of the small-amplitude approximation used in the theoretical analysis. The oscillations at low η are consistent with the oscillations observed to values as low as $\eta = 0.21$ on the analog computer. The peak-to-peak amplitude usually reached a minimum in the frequency range of 10^3 to 10^4 hertz. At this minimum value the frequency peak on the spectrum analyzer was distinguished from noise only with difficulty. This is the principal reason why the data in this frequency range in figures 9, 11, 14, and 16 have more spread about the best-fitting straight line than the data at higher or lower frequencies.

When the fluctuations in the light output were fed into a spectrum analyzer, the peak representing the fundamental frequency of oscillation was quite narrow in relation to its height for certain conditions of operation. Cases were observed for which the half-amplitude bandwidth of the oscillation peak was 5 percent or less of the center
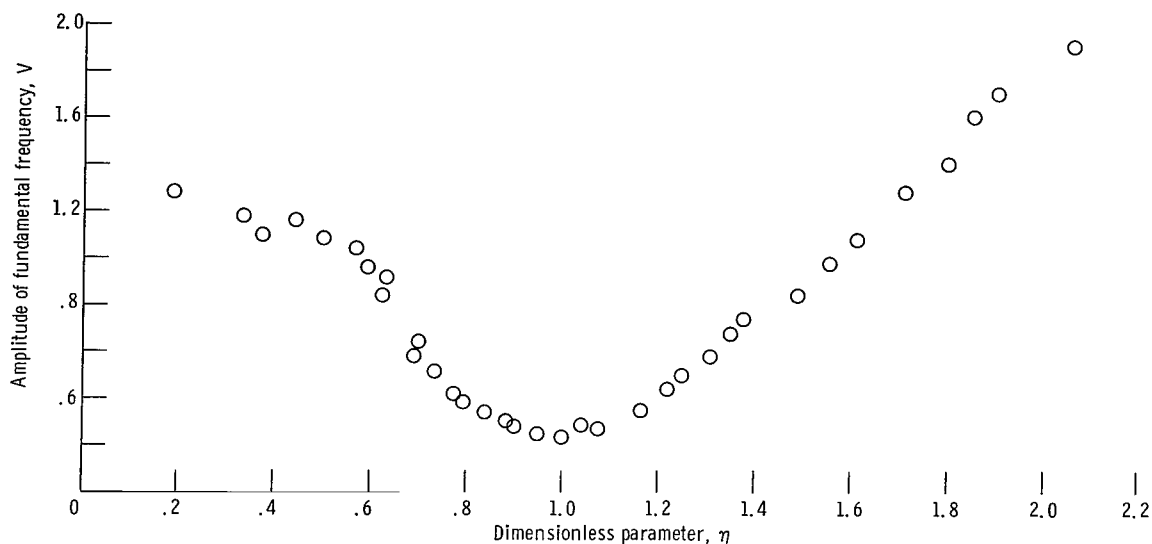
Figure 21. - Observed behavior of peak-to-peak amplitude of $n_e(t)$ as function of parameter proportional to η (given by eq. (28)). Deuterium gas; I_a/v_{obs}^2 normalized to 1 where peak-to-peak amplitude is minimum; runs CO1 to CP11.

frequency of oscillation. This result would not be expected if the magnetic field in the discharge played any role in determining the frequency of oscillation, since the magnetic field varied over more than a factor of 2.5 in the discharge volume.

CONCLUSIONS

The principal finding of this report is that the existence of continuity-equation oscillations has been confirmed in a laboratory plasma. The behavior of these oscillations has been systematically studied over a wide range of operating conditions. The experimental evidence obtained is consistent with all the qualitative predictions of the continuity-equation oscillation mechanism. The data exhibit the predicted dependence of frequency on the square root of the product of mean electron and neutral number density $\sqrt{\tilde{n}_e n_0}$; frequency was independent of magnetic field strength B over more than a factor of 2 in B; the waveform of light fluctuations was cuspoid, with the sharp maxima and broad, flat minima suggestive of a Jacobian elliptic function dependence of the charged-particle density on time; and the peak-to-peak amplitude of oscillation displayed the predicted large values at either extreme of the operating range, with a minimum for intermediate values of a parameter proportional to η.

Only two significant departures from the simple theoretical model were observed. As shown in figures 10, 13, and 17, the frequency is a function of magnetic field

strength below about 0.5 tesla. It is the author's belief that a magnetic-field-dependent diffusion process may be dominant at these low magnetic fields. A second departure from the theoretical model occurs if typical values of frequency of oscillation ν, average neutral number density n_o, and mean electron number density $\tilde{n}_e$ from table I are substituted into equation (29). The effective ionization-rate parameter $\langle \sigma v \rangle_{ne}$ so calculated is about one order of magnitude higher than the electron-neutral ionization-rate parameters quoted in references 12 and 13, for example. The reason for this is not known but is consistent with many experimental studies of magneto-hydrodynamic (MHD) generators and partly ionized plasmas in which much more ionization is found than can be strictly accounted for by known direct electron-neutral ionization processes. Other known oscillatory mechanisms can be ruled out because they do not have the correct functional dependence on $\tilde{n}_e$, n_o, and magnetic field $\underline{B}$, and/or do not span the range of frequencies observed in this experiment.

The generally good qualitative agreement of the experimental data with the simple physical model represented by equations (1) and (2) permits the conclusion that the essential behavior and characteristics of the continuity-equation oscillation are adequately described by these simplified continuity equations, at least for the experimental conditions used herein. The qualitative and quantitative (where obtainable in this experiment) agreement of the data with the closed-form expressions provided by the small-amplitude approximation has shown that the small-amplitude approximation to equations (1) and (2) provides a generally satisfactory theoretical approach to studying the characteristics and behavior of the continuity-equation oscillation.

Lewis Research Center,
    National Aeronautics and Space Administration,
        Cleveland, Ohio, July 30, 1968,
            129-02-03-05-22.

APPENDIX A

SYMBOLS

A	area of energy analyzer aperture
A_i	surface area of plasma across which ions are lost
A_p	total surface area of plasma
B	magnetic field strength, T
E	best-fitting exponent, defined by eq. (34)
$\underline{\mathscr{E}}$	electric field
e	electronic charge, 1.6×10^{-19} C/kg
$G(\eta)$	frequency parameter given by eq. (18)
G_o	geometry factor
$H(\eta)$	frequency parameter given by eq. (22)
I	collector current
I_a	anode current, given by eq. (27), A
I_1	initial current on retarding-potential curve, A
$K(k)$	complete elliptic integral of first kind
k^2	elliptic modulus
l	half width of discharge
n	instantaneous neutral number density
$\tilde{n}$	time-averaged neutral number density
$n(t)$	neutral number density as function of time
$\delta n(t)$	small peak-to-peak perturbation of neutral number density
n_e	instantaneous electron number density
$\tilde{n}_e$	mean electron number density, averaged over a cycle of oscillation
$n_e(t)$	electron number density as function of time
n_{eo}	initial value of $n_e(t)$ at $t = 0$
$n_{e,max}$	maximum value of $n_e(t)$
Δn_e	peak-to-peak amplitude of electron density fluctuation

n_i	ion number density
n_o	time- and space-averaged neutral number density
R	characteristic radius of discharge
SN	Jacobian elliptic sine
T	period of oscillation
t	time
$t_{o,l}$	transit time defined by eq. (B8)
$t_{o,r}$	transit time defined by eq. (B9)
V	total volume of discharge inside area A_p
V_o	kinetic temperature of ions, eV
V_1	potential at which plasma is floating
v	neutral-particle velocity
$\underline{v}$	velocity field
v_i	ion velocity
v_o	average velocity of neutrals
x	position in slab discharge
Z_2	parameter defined by eq. (13)
Z_3	parameter defined by eq. (14)
α	average fraction of total neutral flux through discharge that interacted in discharge volume during a previous cycle of oscillation
ϵ	attenuation coefficient defined by eq. (B7)
$\tilde{\epsilon}$	averaged absorption coefficient defined by eqs. (B10) and (B11)
ϵ_o	permittivity of free space, 8.854×10^{-12} F/m
η	dimensionless parameter defined by eq. (12)
θ	dimensionless argument of Jacobian elliptic function
θ_o	half angle in velocity space of escape cone
λ_o	mean free path
μ_o	permeability of free space, $4\pi \times 10^{-7}$ H/m
ν	frequency of oscillation, Hz
ν_c	collision frequency

ν_o frequency coefficient given by eq. (33)

ν_obs observed frequency of oscillation, Hz

ν_r reduced frequency, defined by eq. (41)

$\langle \sigma v \rangle_\text{ne}$ ionization-rate coefficient of neutrals by electrons

$\langle \sigma v \rangle_\text{ni}$ ionization-rate coefficient of neutrals by ions

φ_n net particle flux

φ_t total particle flux

ψ parameter defined by eqs. (B12) and (B13)

Subscripts:

l leftward-moving

max   maximum

r   rightward-moving

APPENDIX B

DERIVATION OF NEUTRAL-PARTICLE CONTINUITY EQUATION

In this appendix, the neutral continuity equation given by equation (1) is derived for the slab geometry, under simplified assumptions which make clear the physical processes involved. Consider the one-dimensional slab discharge shown in figure 22, in which neutral molecules are streaming into the discharge from the right and left. Electrons of density $n_e(t)$ are streaming along magnetic field lines normal to the plane of the diagram. It is assumed that the mean free path for the electron-neutral ionization process is longer than the width $2l$ of the discharge, so that a diffusion approximation is not appropriate. The neutral-particle continuity equation may be written

$$\dot{n} = -\nabla \cdot \varphi_n - nn_e \langle \sigma v \rangle_{ne} \tag{B1}$$

where $nn_e \langle \sigma v \rangle_{ne}$ represents the loss of neutrals due to ionization by the fast electrons and the source term is the spatial gradient of the net flux at a point x in the discharge. The rightward-moving flux reaching the left-hand boundary is equal to

$$\varphi_r = \frac{1}{2} n_o v \qquad x < -l \tag{B2}$$

and the flux moving to the left beyond $x = l$ is

$$\varphi_l = \frac{1}{2} n_o v \qquad x > l \tag{B3}$$
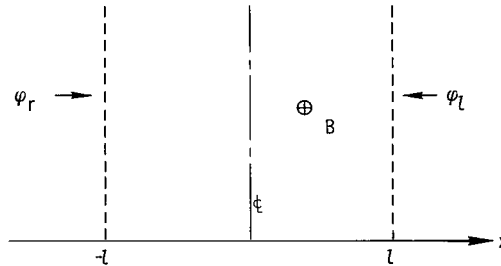
Figure 22. - One-dimensional slab discharge.

where n_o is the average neutral number density in the plenum outside the discharge and v is the velocity of the neutral particles which is assumed to be fixed at one value for the present.

If these fluxes are attenuated exponentially within the discharge with an attenuation coefficient ϵ, the rightward-moving flux inside the discharge may be written

$$\varphi_r = \frac{1}{2} n_o v e^{-\tilde{\epsilon}_r (x+l)} \qquad -l \leq x \leq l \qquad \text{(B4)}$$

and the flux moving to the left is

$$\varphi_l = \frac{1}{2} n_o v e^{-\tilde{\epsilon}_l (l-x)} \qquad -l \leq x \leq l \qquad \text{(B5)}$$

It is important to realize that the attenuation coefficients $\tilde{\epsilon}_r$ and $\tilde{\epsilon}_l$ are not the instantaneous values existing at point x and time t. Since the neutral particles have moved across the discharge, these attenuation coefficients must be averaged over the transit time of the particles in the discharge. The collision frequency of neutrals with electrons is

$$\nu_c = n_e \langle \sigma v \rangle_{ne} \qquad \text{(B6)}$$

The instantaneous value of the attenuation coefficient is the inverse of the mean free path λ_o of a neutral of velocity v, given by

$$\epsilon = \frac{1}{\lambda_o} = \frac{\nu_c}{v} = \frac{n_e \langle \sigma v \rangle_{ne}}{v} \qquad \text{(B7)}$$

The number density n_e is time dependent and must be integrated over the transit times appropriate for rightward-moving or leftward-moving particles. The transit time for rightward-moving particles is

$$t_{o,r} = \frac{l + x}{v} \qquad \text{(B8)}$$

and for leftward-moving particles is

44

$$t_{o,l} = \frac{l - x}{v} \tag{B9}$$

The attenuation coefficients averaged over the transit time they have been in the discharge are, using equations (B7) to (B9),

$$\tilde{\epsilon}_r = \frac{1}{t_{o,r}} \int_{t-t_{o,r}}^{t} \frac{n_e \langle \sigma v \rangle_{ne}}{v} dt' = \frac{\langle \sigma v \rangle_{ne}}{l + x} \int_{t-t_{o,r}}^{t} n_e \, dt' \tag{B10}$$

and

$$\tilde{\epsilon}_l = \frac{\langle \sigma v \rangle_{ne}}{l - x} \int_{t-t_{o,l}}^{t} n_e \, dt' \tag{B11}$$

since $\langle \sigma v \rangle_{ne}$ and v are, by hypothesis, not functions of time. The following quantities are defined:

$$\psi_r \equiv (l + x)\tilde{\epsilon}_r = \langle \sigma v \rangle_{ne} \int_{t-t_{o,r}}^{t} n_e \, dt' \tag{B12}$$

and

$$\psi_l \equiv (l - x)\tilde{\epsilon}_l = \langle \sigma v \rangle_{ne} \int_{t-t_{o,l}}^{t} n_e \, dt' \tag{B13}$$

The total neutral flux $\varphi_t(x, t)$ inside the discharge may be written, using equations (B4), (B5), (B12), and (B13), as

$$\varphi_t = \varphi_r + \varphi_l = nv = \frac{1}{2} n_o v \left(e^{-\psi_r} + e^{-\psi_l} \right) \tag{B14}$$

and the effective total density in the discharge is

$$n(x, t) = \frac{1}{2} n_o \left(e^{-\psi_r} + e^{-\psi_l} \right) \tag{B15}$$

The net flux, with rightward-moving flux considered positive, is given by the difference of the two fluxes, or

$$\varphi_n = \varphi_r - \varphi_l = \frac{1}{2} n_o v \left(e^{-\psi_r} - e^{-\psi_l} \right) \tag{B16}$$

The divergence of this quantity, required in the continuity equation, is

$$-\nabla \cdot \varphi_n = \frac{1}{2} n_o v \left(\frac{\partial \psi_r}{\partial x} e^{-\psi_r} - \frac{\partial \psi_l}{\partial x} e^{-\psi_l} \right) \tag{B17}$$

When equations (B12) and (B13) are used, the derivatives are

$$\frac{\partial \psi_r}{\partial x} = \frac{\langle \sigma v \rangle_{ne}}{v} n_e(t - t_{o,r}) \tag{B18}$$

and

$$\frac{\partial \psi_l}{\partial x} = -\frac{\langle \sigma v \rangle_{ne}}{v} n_e(t - t_{o,l}) \tag{B19}$$

where $t_{o,r}$ and $t_{o,l}$ are functions of x. Equation (B17) can then be written

$$-\nabla \cdot \varphi_n = \frac{1}{2} n_o \langle \sigma v \rangle_{ne} \left[n_e(t - t_{o,r}) e^{-\psi_r} + n_e(t - t_{o,l}) e^{-\psi_l} \right] \tag{B20}$$

To simplify the following analysis, attention is restricted to the midplane of the slab, where $x = 0$, so that $\psi_r = \psi_l = \psi$; $t_o = t_{o,l} = t_{o,r} = l/v$. From equation (B15),

$$n(0, t) = n = n_o e^{-\psi} \tag{B21}$$

46

and equation (B20) becomes

$$-\nabla \cdot \varphi_n = n_o e^{-\psi} \langle \sigma v \rangle_{ne} n_e (t - t_o) = n \langle \sigma v \rangle_{ne} n_e \left(t - \frac{l}{v} \right) \qquad (B22)$$

Substituting equation (B22) into equation (B1) results in the following form of the continuity equation:

$$\dot{n} = n \langle \sigma v \rangle_{ne} \left[n_e \left(t - \frac{l}{v} \right) - n_e(t) \right] \qquad (x = 0) \qquad (B23)$$

The source term in this continuity equation is therefore characteristic of the retarded time $t - t_o$. It is this decoupling and averaging that is responsible for the continuity-equation relaxation oscillations.

When the neutral molecules have a Maxwellian distribution of velocities, the transit time $t_o = l/v$ will vary over a wide range $0 \leq t_o \leq \infty$, and the retarded value of the electron number density can therefore be replaced with its average value over a period of oscillation. There will always be some particles with nearly zero velocities that will be present in the discharge for a period or longer, so

$$n_e \left(t - \frac{l}{v} \right) \approx \frac{1}{T} \int_0^T n_e(t')dt' \approx \tilde{n}_e \qquad (B24)$$

where T is the period of oscillation. Since the average neutral influx is equal to the average electron efflux, the coefficients of the source term in equations (B23) and (1) can be related to obtain

$$\frac{\alpha A_p v}{4V} = \tilde{n}_e \langle \sigma v \rangle_{ne} \qquad (B25)$$

It can be shown by a similar argument that the charged-particle continuity equation (eq. (2)) can be written

$$\dot{n}_e = -n_e(t)n_o \langle \sigma v \rangle_{ne} + n_e(t)n(t) \langle \sigma v \rangle_{ne} \qquad (B26)$$

47

where n_o is the time-averaged neutral number density. The first term of the right side of equation (B26) can be obtained from the divergence term

$$-\nabla \cdot n_e \rightarrow n_e(t)n_o \langle \sigma v \rangle_{ne} \tag{B27}$$

with the same argument by changing variables, n_e to n and n to n_e, and by realizing that the exponentials in equations (B4) and (B5) are positive, since the ionization process leads to an enhancement of $\tilde{n}_e$ in the discharge region.

APPENDIX C

WAVEFORMS OF PERIODIC SOLUTIONS

For the benefit of those not familiar with the Jacobian elliptic functions, the waveforms of equations (15) and (19) have been calculated as a function of η, and selected examples are illustrated in figure 23. Illustrated are normalized graphs of equation (15) $(2/3 \leq \eta \leq 1.0)$ and of equation (19) $(\eta \geq 1.0)$ as functions of the argument $\theta = 2K(k)\nu t$ for the following values of η: 0.6667, 0.667, 0.670, 0.75, 0.95, 1.10, 1.60, 50.0, and 500.0. Note the increase in peak-to-peak amplitude and characteristic Jacobian waveform as η approaches the ends of its range. When $\eta = 1.0$, the equations (1) and (2) represent a nonoscillating steady state.
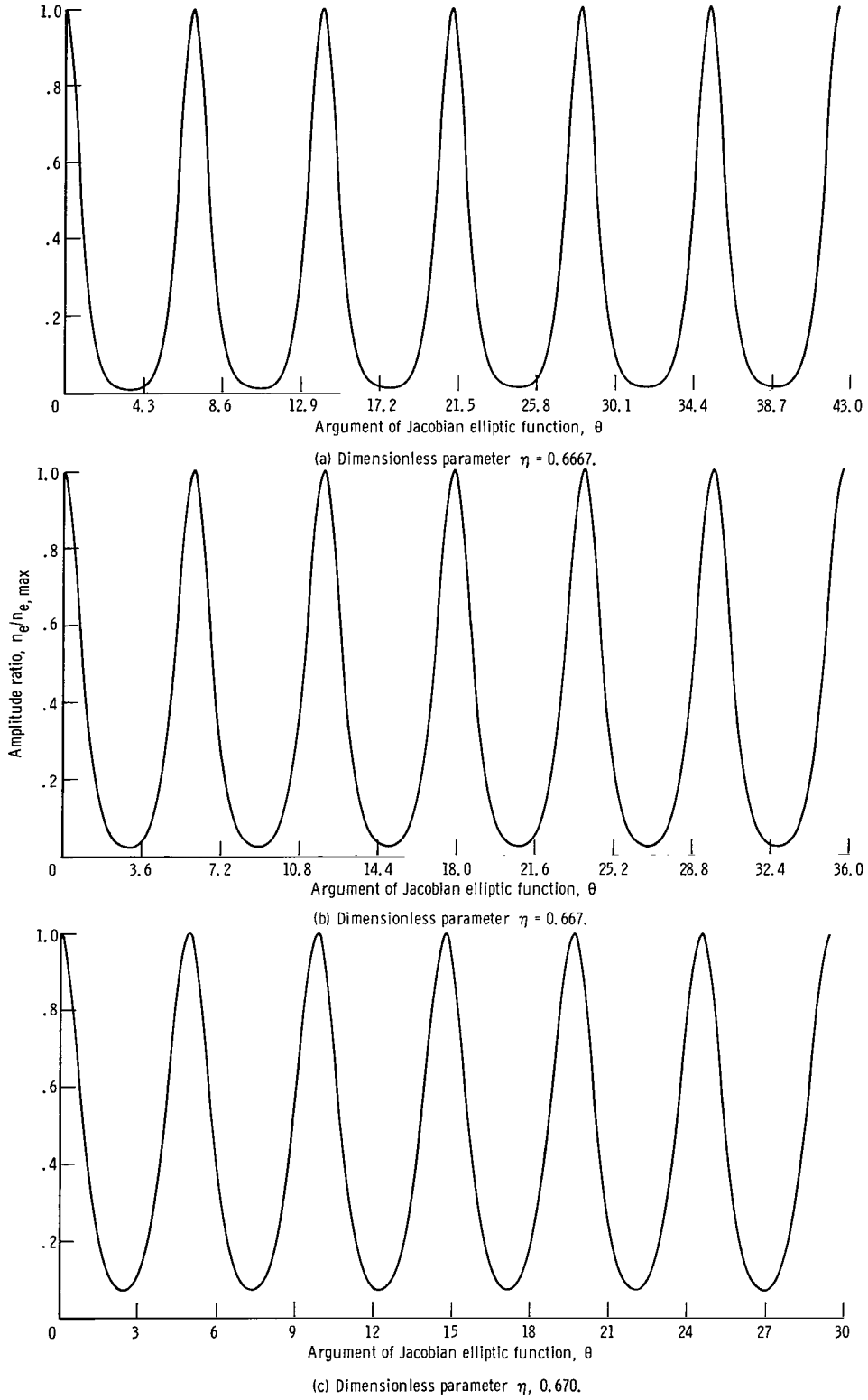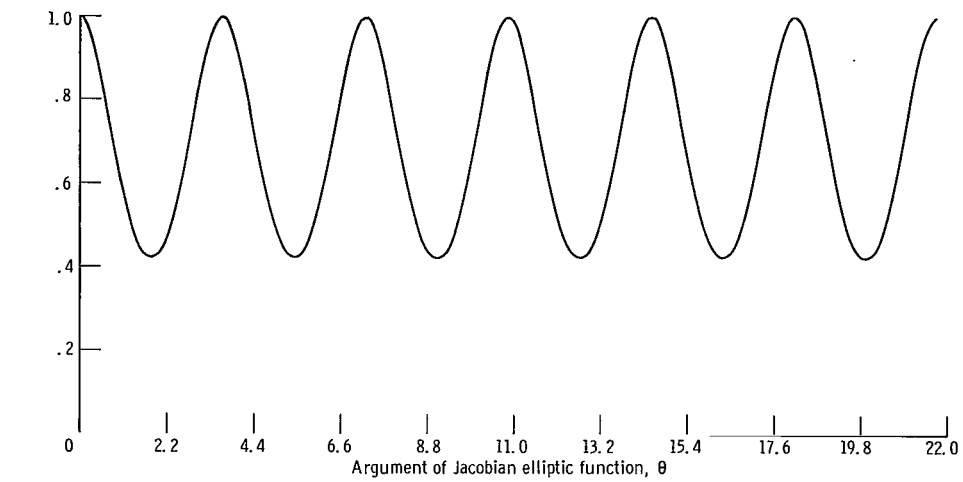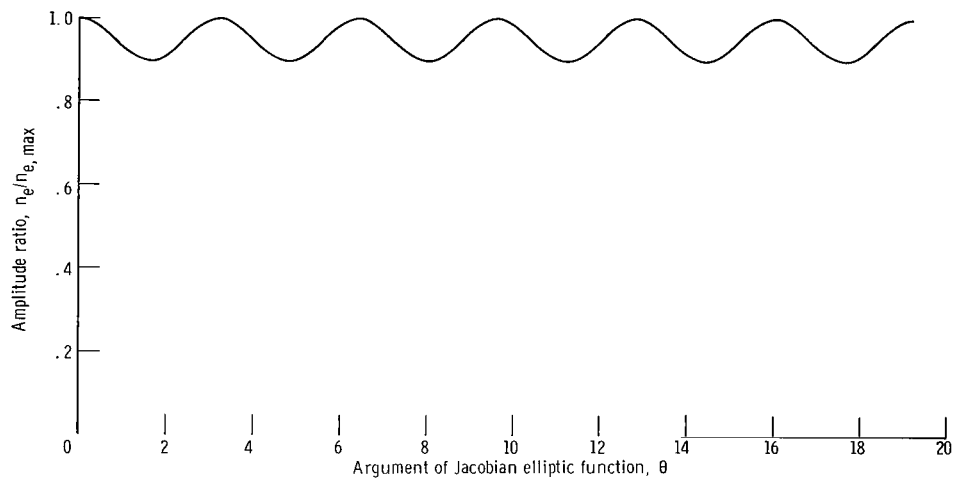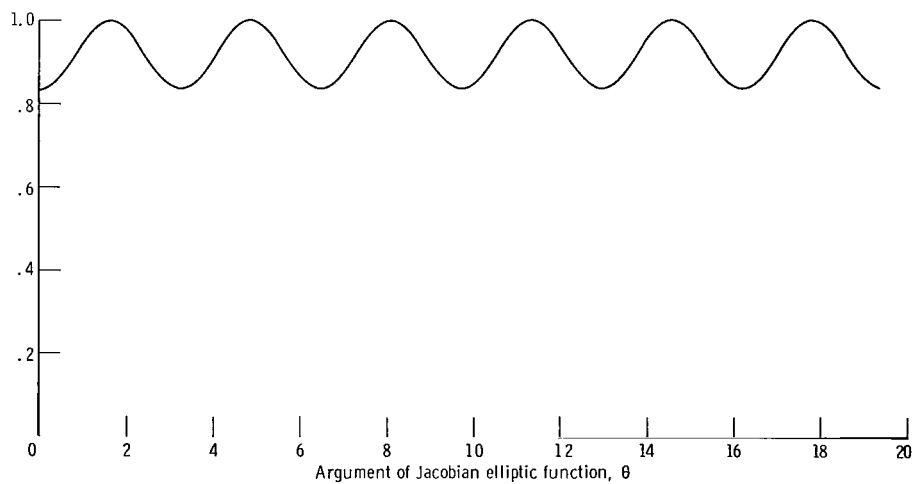
(a) Dimensionless parameter $\eta = 0.6667$.

(b) Dimensionless parameter $\eta = 0.667$.

(c) Dimensionless parameter η, 0.670.

Figure 23. – Waveforms of periodic solutions.

50

(d) Dimensionless parameter, η, 0.75.

(e) Dimensionless parameter η = 0.95.

(f) Dimensionless parameter η = 1.10.

Figure 23. - Continued.

51

(g) Dimensionless parameter $\eta = 1.60$.

(h) Dimensionless parameter $\eta = 50.0$.
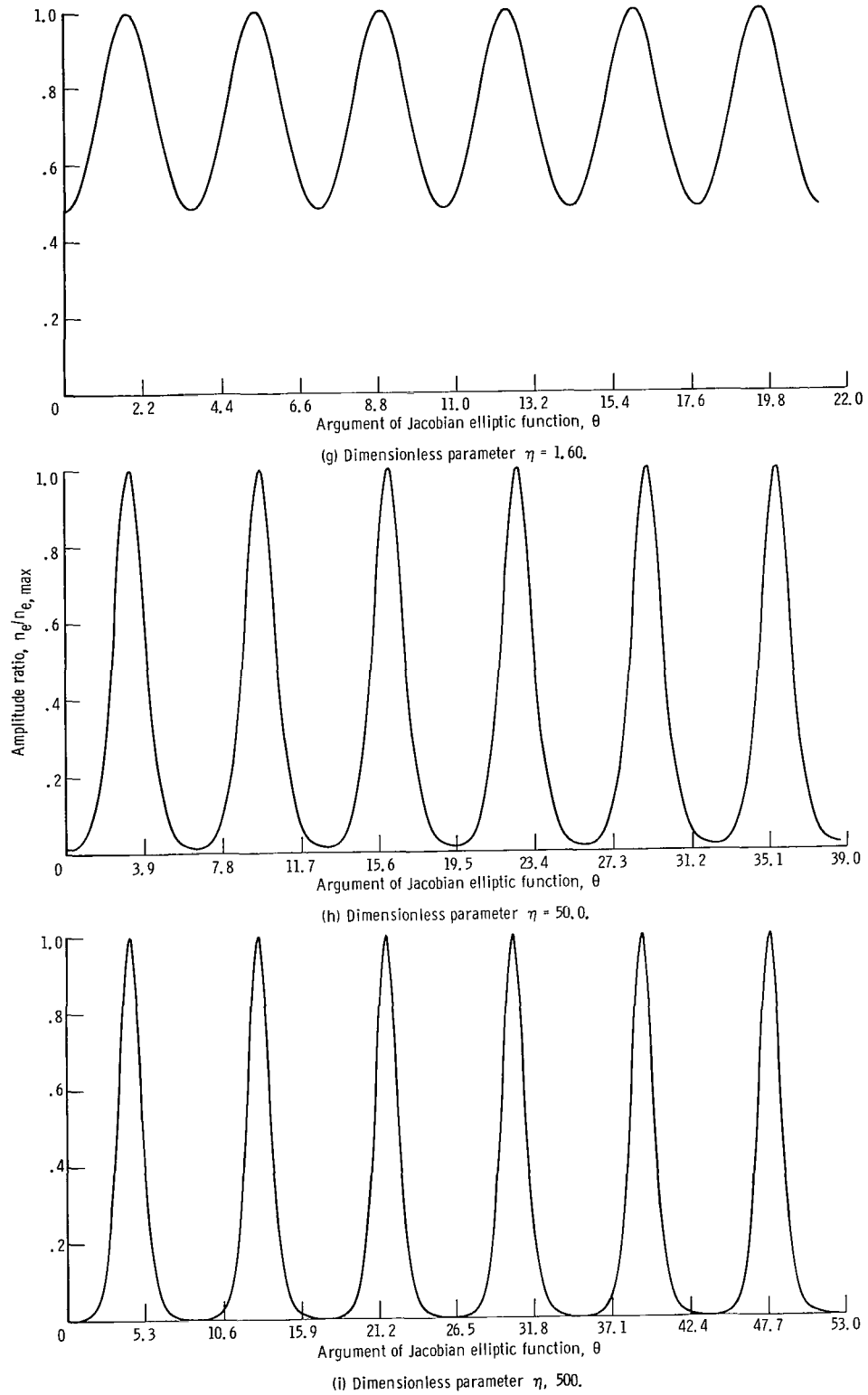
(i) Dimensionless parameter η, 500.

Figure 23. - Concluded.

REFERENCES

1. Lehnert, B.: Experimental Evidence of Plasma Instabilities. Plasma Phys., vol. 9, 1967, pp. 301-337.

2. Roth, J. Reece: Modification of Penning Discharge Useful in Plasma Physics Research. Rev. Sci. Instr., vol. 37, no. 8, Aug. 1966, pp. 1100-1101.

3. Roth, J. Reece: A New Mechanism for Low-Frequency Oscillations in Partially Ionized Gases. Phys. Fluids, vol. 10, no. 12, Dec. 1967, pp. 2712-2714.

4. Robertson, Harry S.: Moving Striations in Direct Current Glow Discharges. Phys. Rev., vol. 105, no. 2, Jan. 15, 1957, pp. 368-377.

5. Gentle, Kenneth W.: Moving Striations in the Argon Positive Column, I. Theory. Phys. Fluids, vol. 9, no. 11, Nov. 1966, pp. 2203-2211.

6. Lotka, Alfred J.: Undamped Oscillations Derived from the Law of Mass Action. J. Am. Chem. Soc., vol. 42, no. 8, Aug. 1920, pp. 1595-1599.

7. Volterra, V.: Variations and Fluctuations of the Number of Individuals in Animal Species Living Together. International Council for the Exploration of the Sea. Journal du Counseil, vol. 3, 1928, pp. 1-51.

8. Roth, J. Reece: Periodic, Small-Amplitude Solutions to the Spatially Uniform Plasma Continuity Equations. NASA TN D-4472, 1968.

9. Roth, J. Reece: A New Mechanism for Low-Frequency Oscillations in Partially Ionized Gases. Paper presented at the Eighth International Conference on Ionization Phenomena in Gases, Vienna, Austria, Aug. 27 - Sept. 2, 1967.

10. Davis, Harold T.: Introduction to Nonlinear Differential and Integral Equations. Dover Publications, Inc., 1962, p. 129.

11. Byrd, P. F.; and Friedman, M. D.: Handbook of Elliptic Integrals for Engineers and Physicists. Springer-Verlag, Berlin, 1954.

12. Lotz, Wolfgang; Electron-Impact Ionization Cross-Sections and Ionization Rate Coefficients for Atoms and Ions. Astrophys. J. Suppl. Ser., vol. 14, no. 128, May 1967, pp. 207-238.

13. Lotz, Wolfgang: Electron Impact Ionization Cross-Sections and Ionization Rate Coefficients for Atoms and Ions from Hydrogen to Calcium. Rep. IPP-1/62, Institut für Plasmaphysik G.m.b.H, May 1967.

14. Roth, J. Reece; Freeman, Donald C. Jr.; and Haid, David A.: Superconducting Magnet Facility for Plasma Physics Research. Rev. Sci. Instr., vol. 36, no. 10, Oct. 1965, pp. 1481-1485.

15. Roth, J. Reece: Steady-State, Hot-Ion Particle Injection Scheme for Mirror Machines. Bull. Am. Phys. Soc., vol. 11, no. 4, June 1966, p. 465.

16. Roth, J. Reece; and Clark, Marion: Analysis of Integrated Charged Particle Energy Spectra from Gridded Electrostatic Analyzers. NASA TN D-4718, 1968.

17. Fedorenko, N. V.: Ionization in Collisions Between Ions and Atoms. Soviet Phys.-Uspekhi, vol. 2, no. 4, July-Aug. 1959, pp. 526-546.

18. Gilbody, H. B.; and Hasted, J. B.: Ionization by Positive Ions. Proc. Roy. Soc. (London), ser. A, vol. 240, no. 1222, June 11, 1957, pp. 382-395.

19. Polman, J.; Phillipo, T. J.; and Van Der Werf, J. E.: Diagnostics of Low-Density Plasmas by Means of a 4 MM Lecher Wire Microwave Interferometer. Paper 5.4.3, Eighth Internation Conference on Phenomena in Ionized Gases, Vienna, Austria, 1967, p. 498.

"The aeronautical and space activities of the United States shall be conducted so as to contribute . . . to the expansion of human knowledge of phenomena in the atmosphere and space. The Administration shall provide for the widest practicable and appropriate dissemination of information concerning its activities and the results thereof."

— NATIONAL AERONAUTICS AND SPACE ACT OF 1958

NASA SCIENTIFIC AND TECHNICAL PUBLICATIONS

TECHNICAL REPORTS: Scientific and technical information considered important, complete, and a lasting contribution to existing knowledge.

TECHNICAL NOTES: Information less broad in scope but nevertheless of importance as a contribution to existing knowledge.

TECHNICAL MEMORANDUMS: Information receiving limited distribution because of preliminary data, security classification, or other reasons.

CONTRACTOR REPORTS: Scientific and technical information generated under a NASA contract or grant and considered an important contribution to existing knowledge.

TECHNICAL TRANSLATIONS: Information published in a foreign language considered to merit NASA distribution in English.

SPECIAL PUBLICATIONS: Information derived from or of value to NASA activities. Publications include conference proceedings, monographs, data compilations, handbooks, sourcebooks, and special bibliographies.

TECHNOLOGY UTILIZATION PUBLICATIONS: Information on technology used by NASA that may be of particular interest in commercial and other non-aerospace applications. Publications include Tech Briefs, Technology Utilization Reports and Notes, and Technology Surveys.

Details on the availability of these publications may be obtained from:

SCIENTIFIC AND TECHNICAL INFORMATION DIVISION

NATIONAL AERONAUTICS AND SPACE ADMINISTRATION
Washington, D.C. 20546